Investigation of biodegradable metal for Urological Applications

by

ALLISON YINETH RODRIGUEZ MARTINEZ

Undergraduate Project

Tutor

Prof. Inġ. Joseph Buhagiar

Prof. Inġ. Bertram Mallia

PhD. Marcela Cristina Múnera Ramírez

UNIVERSIDAD DEL ROSARIO

ESCUELA COLOMBIANA DE INGENIERÍA JULIO GARAVITO

BIOMEDICAL ENGINEERING PROGRAM

BOGOTÁ D.C

2020

UNIVERSITY OF MALTA

Faculty of Engineering

Department of Metallurgy and Materials Engineering

FINAL YEAR PROJECT

B.ENG (Hons.)

Investigation of biodegradable metal for Urological Applications

by

Allison Yineth Rodriguez Martinez

A dissertation submitted in partial fulfilment of the requirements of the award of Bachelor of Engineering (Hons.) of the University of Malta

June 2020

L-Università ta' Malta

FACULTY/INSTITUTE/CENTRE/SCHOOL Faculty of Engineering.

DECLARATIONS BY UNDERGRADUATE STUDENTS

Student's Code 1903872.

Student's Name & Surname Allison Yineth Rodriguez Martinez.

Course Bachelor of Engineering (Hons).

Title of Long Essay/Dissertation Investigation of biodegradable metal for urological applications.

Word Count 21384.

(a) Authenticity of Long Essay/Dissertation

I hereby declare that I am the legitimate author of this Long Essay/Dissertation and that it is my original work.

No portion of this work has been submitted in support of an application for another degree or qualification of this or any other university or institution of higher education.

I hold the University of Malta harmless against any third party claims with regard to copyright violation, breach of confidentiality, defamation and any other third party right infringement.

(b) Research Code of Practice and Ethics Review Procedures

I declare that I have abided by the University's Research Ethics Review Procedures. Research Ethics & Data Protection form code _____.

Allison Rodriguez.
Signature of Student

ALLISON Y. RODRIGUEZ.
Name of Student (in Caps)

COPYRIGHT NOTICE

1) Copyright in text of this dissertation rests with the Author. Copies (by any process) either in full, or of extracts may be made only in accordance with regulations held by the Library of the University of Malta. Details may be obtained from the Librarian. This page must form part of any such copies made. Further copies (by any process) made in accordance with such instructions may not be made without the permission (in writing) of the Author.

2) Ownership of the right over any original intellectual property which may be contained in or derived from this dissertation is vested in the University of Malta and may not be made available for use by third parties without the written permission of the University, which will prescribe the terms and conditions of any such agreement."

ABSTRACT

To avoid a second surgery to remove ureteral stents, degradable metals have been studied. Since Fe and Mg alloys have not shown an adequate combination of biocompatibility and degradation rate *in vivo* and *in vitro*, in the present work, the Zn based samples were investigated as potential biodegradable material for ureteral stent application.

In this study, the characterisation of mechanical properties, determination of the degradation resistance under artificial urine (AU) for electrochemical and immersion tests, and analysis of the elemental composition of the corrosion layer were carried out in pure Zn samples (wire and sheet).

The corrosion rate of Zn in the electrochemical test was 0.10 ± 0.04 mm/year. In contrast, the corrosion rate in immersion test under a period of one day and three days were 0.08 (+0.45 and -0.24) mm/year and -0.20 (+0.41 and -0.01) mm/year, respectively. However, the corrosion rates implied a slower degradation ratio than the results of other studies with pure Zn samples.

The corrosion rates obtained were affected by the presence of the ZnO. Non uniform corrosion of Zn was observed and Ca in the corrosion layer is an undesirable result. Moreover, the diameter reduction for Zn wire samples displayed a relationship between mass loss and immersion time.

This work shows significant results to take account in further studies in the urological field; however, mechanical properties and corrosion behaviour of pure Zn samples need to be improved.

Acknowledgements

Foremost, I would like to express my gratitude towards my project supervisor Prof. Inġ. Joseph Buhagiar and co-supervisors Prof. Inġ. Bertram Mallia and PhD. Marcela Múnera, who constantly provided guidance, encouragement, and support during the execution of the project. Also, my sincere gratitude for the attention given to my safe return to Colombia under the COVID-19 situation.

Specially thanks to all members of the Department of Metallurgy and Materials laboratory, Inġ. James Camilleri, Inġ. Mary Grace Micallef, Mr. Nicholas Gingell, and Mr. Daniel Dimech, for their continuous assistance, invaluable technical support, company during my stay in Malta and their help in the remote sessions' lab. I would also like to show my gratitude to Christabelle Tonna, Antonino Mazzonello, Jeanelle Arpa, and Eleanor Saliba for their support and availability to accompany me to laboratory practices. I would also like to give my thanks to Prof. William Rodriguez, the University of Rosario (Colombia), and the University of Malta to give me the opportunity of learning about biomaterials and live a new experience.

I am also grateful to my closest friends form Colombia and Malta to keep support during the development of this project.

Finally, this thesis would not have been possible without the support and love of the people nearest to my heart, my parents, Samuel and Nelly, and my brother Samuel Ricardo.

Contents

Contents v

List of Tables vii

List of Figures viii

List of Abbreviations x

Introduction 1

Literature Review 3

2.1 The Urinary System 3

2.1.1 Kidneys and ureters 3

2.1.2 Urine 4

2.2 Artifical urine (AU) 5

2.3 Urinary tract obstruction 6

2.4 Ureteric stents 7

2.4.1 Stents complications 8

2.4.2 Engineering solutions 9

2.5 Ureteric stent designs 10

2.6 Urological applications materials 13

2.6.1 Polymers 13

2.6.2 Metals 15

2.7 Zinc 16

2.7.1 Toxicological aspects of Zn 16

2.7.2 Mechanical properties of conventional and absorbable Zn-based alloys 17

2.7.3 Corrosion behaviour and biodegradability of Zn-based alloys 19

2.8 Techniques for electrochemical degradation 24

2.8.1 Open circuit potential (OCP) 24

2.8.2 Potentiodynamic polarisation (PDP) 25

Materials and Methods 27

3.1 Material specification and characterisation 27

3.2 AU solution preparation 28
3.3 Vickers microhardness test 29
3.4 Corrosion testing 29
3.4.1 *In vitro* degradation testing, Zn sheet samples 29
3.4.2 *In vitro* degradation testing, Zn wire samples 31

Results **35**
4.1 Characterisation of Zn samples prior corrosion testing 35
4.2 Microhardness test 37
4.3 Set-up used in the immersion test 38
4.4 AU solution 38
4.5 Electrochemical corrosion analysing test 39
4.6 Immersion corrosion analysing test 45

Discussion **51**
5.1 Zn samples Degradation Resistance 51
5.2 Elemental composition of the corrosion layer of Zn samples 52
5.3 Mechanical properties of the Zn samples 53
5.4 AU solution 54
5.5 Set-up used in the immersion test 54

Conclusion **56**

Future medium-term works **58**

References **59**

List of Tables

Table 1. Physiological ranges of selected compounds in healthy human urine. Adapted from [10, 13, 16]. 5

Table 2. Mechanical properties of pure Zn and Zn alloys. Adapted from [94]. 18

Table 3. Degradation rates of different Zn and Zn-based alloys form immersion (CRI) and electrochemical (CRE) tests. Adapted from [94]. 22

Table 4. AU solution composition brought to 500 ml by adding distilled H_2O (diH_2O) and tris solution. 28

Table 5. Design criteria for set-up for *in vitro* degradation for Zn wire samples. 31

Table 6. Elemental composition of Zn samples as received. 35

Table 7. Corrosion parameters calculated from the potentiodynamic curves. 41

Table 8. Elemental composition (wt. %) of corrosion products, n =4 of Zn sheet samples after polarisation test. Typical zones showed in Figure 19(d); average and standard deviation. 42

Table 9. Elemental composition (wt. %) of corrosion products of Zn after polarisation test. Zones showed in Figure 21. 43

Table 10. Corrosion rate of n=3 samples of wire for each immersion time (1 day and 3 days); average data and range as error. 45

Table 11. Composition obtained in EDS areas along the wire in the immersion test (1 day and 3 days samples) as a function of zones A, B and C shown in the Figure 25 and Figure 26. Data expressed as: average value and standard deviation of n = 24. 50

Table 12. p-values from T-student* or U-mann Withney testing of comparison of the composition obtained in each zone along the wire as function of the immersion time. p-values>0.05 implies that no difference can be observed between the two datasets being compared. 50

Table 13. p-values from T-student* or U-mann Withney testing of comparison between composition of zone A and zone C obtained in EDS along the wire in the immersion test where p-values>0.05 implies that no difference can be observed between the two datasets being compared. 50

List of Figures

Figure 1. The scheme of normal urinary system anatomy [8]..... 3

Figure 2. Ureter shapes on human anatomy. The ureter was (a) tubular, (b) funnel-shaped, or (c) undulated [11]..... 4

Figure 3. Upper and lower urinary tract causes and sites of obstruction [22]..... 7

Figure 4. Conditioning film, bacterial adhesión and stent encrustation after placement of ureteric stent..... 8

Figure 5. Stent architecture evolution through years. 12

Figure 6. Pourbaix diagram of Zn [94]. 21

Figure 7. Example of Tafel extrapolation, corrosion of metal in acidic aqueous medium [143]..... 25

Figure 8. Hypothetical cathodic and anodic polarisation plot for determining localized corrosion parameters [142]. 26

Figure 9. Schematic of the AU solution preparation..... 29

Figure 10. Schematic illustration of the *in vitro* degradation set-up used to investigate the degradation behaviour of zinc wire samples..... 32

Figure 11. Final schematic diagram of (a) the set-up to immersion test. Blue arrows show direction of the flow or the AU artificial urine. (b) position of Zn wire sample in the simulated ureter. 33

Figure 12. Diffractogram of as-received Zn sheet sample and Zn wire sample..... 36

Figure 13. SEM image of the surface of Zn wire sample as received..... 37

Figure 14. Comparison of Vickers microhardness results of study 1 (ref. [93]), study 2 (ref. [105]), study (ref. [108]) and this study. 37

Figure 15. Result of the AU solution under the same protocol. (a) Powder chemicals were not crushed enough, (b) ideal AU solution, (c) Tris solution added on the chemical powder mixture and (d) the HCl used was contaminated..... 38

Figure 16. Results of pH of prior and after immersion test (a) Reference colour bar of the Universal Indicator Paper pH 1-14, (b) results over 1 day, (c) results over 3 days. 39

Figure 17. OCP plots of the n = 4 Zn sheet samples, in artificial urine solution. Potential vs. time. 40

Figure 18. Potentiodynamic plots of n = 4 Zn sheet samples in artificial urine solution. Current density vs. potential..... 41

Figure 19. SEM images showing the typical diameter of the circumferences produced by the AU solution on Zn sheet samples after polarisation. (a) Inner circumference, Zone A. (b) Intermediate circumference, Zone B. (c) External circumference, Zone C. (d) Location of each EDS area on each zone..... 42

Figure 20. Elemental composition (wt. %) comparison between samples prior test, and zones identified after PDP tests in AU solution regarding to C, O and Zn elements. Average value and standard deviation as error. 43

Figure 21. SEM micrographs showing the surface morphologies of Zn sheet samples after potentiodynamic testing in artificial urine solution and subsequent rinsing and sonication in ethanol at (a-c)500 X. (d) 1K X. (e, f) 2K X and (g) 10K X..... 44

Figure 22. Comparison of corrosion rate obtained in electrochemical tests (CRE) and immersion time (CRI) in 1st day and 3rd days. 45

Figure 23. Average diameter for the zinc wire after 1 and 3 days of immersion test in AU solution, with range as error..... 46

Figure 24. SEM images of corrosion layer develop on the surface of Zn wire samples after immersion test in AU solution, (a, b) 1 day and (c, d) 3 days in two points on the wire: proximal part (part near to the kidney, location in the wire 1) and distal part (part near to the bladder, location in the wire 12). Dotted lines mark the corrosion layer. 47

Figure 25. SEM images showing the typical morphology of (a-d) corrosion layer and (e-h) corrosion products in the boundaries of wire generated in samples in 1 day on immersion test in artificial urine solution. SEM images at 2 KX. Red squares (zone A), yellow squares (zone B) and blue squares (zone C). 48

Figure 26. SEM images showing the typical morphology of (a-d) corrosion layer and (e-h) corrosion products in the boundaries of wire generated in samples in 3 days on immersion test in artificial urine solution. SEM images at 2 KX. Red squares (zone A), yellow squares (zone B) and blue squares (zone C). 49

List of Abbreviations

AU	Artificial Urine
I_{corr}	Corrosion current density, ($\mu A\ cm^{-2}$)
CRI	Corrosion rate for immersion tests, (mm/year)
CRE	Corrosion rate for electrochemical tests, (mm/year)
diH_2O	Distilled water
ρ	Density of zinc, ($7.13\ g\ cm^{-3}$)
EW	Equivalent weigh of zinc, ($32.68\ g\ eq^{-1}$)
A	Exposed surface area, (cm^2)
t	Immersion time, (h)
OCP	Open circuit potential
SRS	Stent-related symptoms
UTI	Urinary tract infection
λ	Wavelength, (nm)
ΔW	Weight change, (g)

Chapter 1

Introduction

Ureteral stents have become an important part of new urological practices, and a lot of studies have been improved biocompatibility, reducing encrustation with modifications in the biofilm formation, infections and stent-related morbidity with long-term use [1].

Some adverse effects with the use of ureteral stents are pain, stent fragmentation and migration, encrustation, and even death [2, 3]. The time that the stent is inside the body promotes the bacterial adhesion and the increase of anchor zone to lead encrustations [4, 5]. Thus, the removal procedure of the stent is the unique alternative to prevent patient's morbidity due to possible complications generated by the ureteral stents [6].

So, a biodegradable ureteral stent would be a breakthrough as it would obviate the need for multiple procedures and would minimise incrustation and other adverse side effects. In the last decade, iron (Fe) and magnesium (Mg) -based alloys have been studied as potential biodegradable metals for medical applications. However, some experiences with these materials reveal critical limitations in terms of mechanical properties and biodegradation behaviour. Recently, Zn-based alloys have been proposed as promising degradable metallic alternatives. One advantage of Zn is that the main degradation product, Zn^{2+}, is presented in the physiological systems and in different biochemical processes [7].

1.1 Objectives

The main aim of this project is the Zn based samples were investigated as potential biodegradables material for stent applications through *in vitro* corrosion testing and surface characterization of the corrosion layer.

(i) Determine the biodegradation rate of the Zn alloy as ureteral stents, on the simulated urological fluid.

Corrosion rates were measured by potentiodynamic polarisation, and immersion tests, for a period of one day and three days using artificial urine solution.

(ii) Characterise corrosion layer after degradation *in vitro* testing:

Corrosion layer characterisation was done using SEM and EDS in order to observe the elemental composition and the thickness of it.

(iii) Development of a set-up to mimetic the ureteral system, considering properties such as: temperature, pH, flow, and chemical substances.

The apparatus designed to simulate the upper urinary tract and perform the immersion tests check the following design criteria: length and diameter of ureter based on healthy men, flow rate of urine through the ureter and body temperature.

(iv) Characterise the mechanical properties of the Zn samples used:

Vickers micro-hardness test was performed in order to evaluate the hardness of the Zn samples employed in this study.

Chapter 2

Literature Review

2.1 The Urinary System

The renal system is made-up of two kidneys, two ureters, a bladder, a urethra, (Figure 1), and striated sphincter. The kidneys produce urine. Urine is stored in the bladder which flows through the ureters. Finally, the urine is carried out of the human body through the urethra and striated sphincter.

The system using urine, eliminates products of the metabolism of the organism and conserve elements such as water, minerals and electrolytes. The urinary system contributes to the homeostasis of the human body [8].

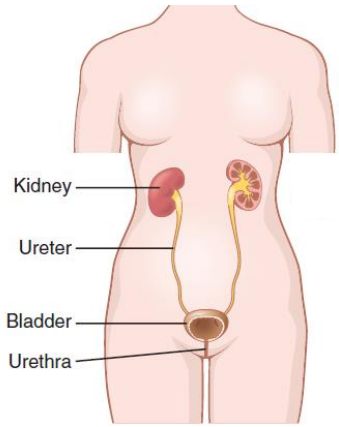

Figure 1. The scheme of normal urinary system anatomy *[8]*.

2.1.1 Kidneys and ureters

The kidneys are located on the ribs and behind the belly, sitting on the posterior abdominal wall. Each kidney is about: 11 cm long, 6 cm wide and 3 cm thick and weighs around 150-160 g [9]. The functions of the kidney generally are to filter the blood,

regulate minerals in human body, maintain body fluid balance, and also produce hormones [8].

On other hand, ureters are 22-30 cm long and thick-walled. Ureteral diameter varies from 1 to 15 mm along the renal pelvis and the urinary bladder [9, 10]. The shape of the whole length of the ureter could be described as a tube, a funnel, or a combination of the two, undulated [11], as shown in the Figure 2.

The flow of urine is contributed by the activity of the muscular walls of the ureters, peristaltic contractions, hydrostatic pressure and gravity [10]. About 1 to 5 peristaltic contractions occur per minute in the ureter [11], causing a bolus of urine [12].

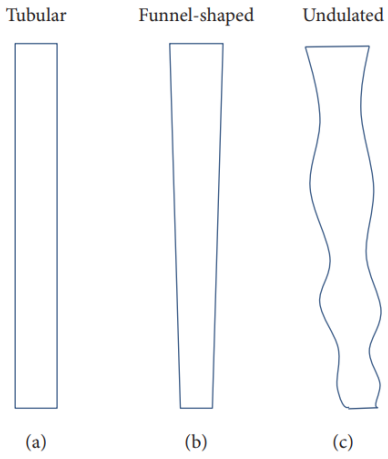

Figure 2. Ureter shapes on human anatomy. The ureter was (a) tubular, (b) funnel-shaped, or (c) undulated *[11]*.

2.1.2 Urine

Through the formation of urine, the volume and physicochemical characteristics of extracellular and intracellular fluid are stabilized. For this, the kidney conserves water and electrolytes present in body fluids, mainly sodium, potassium and chloride; and it eliminates excess water and electrolytes from intake, metabolic waste products (urea, creatinine, hydrogen ions) and, toxic products that may have penetrated the body [9].

However, the amount, composition and ionic strength of human urine can be influenced by factors which include gender, age, race [13], dietary intake, exercise, environmental temperature and medical conditions [14]. Furthermore, urine changes throughout the day in the same person, more concentrated in the morning [15]; making

it difficult to establish normal levels for each compound in the urine. Table 1 shows the physiological ranges of selected compounds and characteristics in healthy human urine.

The physical characteristics of urine are important to identify if the patient is healthy or not. For instance, the colour and odour of the urine are rough descriptors of the hydration state. A healthy human urine is mildly aromatic and transparent when freshly discharged and becomes ammonia-like and turbid (cloudy) on standing. Finally, the pH varies with diet. Acidity in the urine is associated with high-protein diets, while alkalinity is related with vegetarian diets [10, 16].

Table 1. Physiological ranges of selected compounds in healthy human urine. Adapted from *[10, 13, 16]*.

Property and composition	Molar mass (g/mol)	Normal range (reference age in years)
pH		4.5 - 8.0, average 6.0.
Specific gravity (SG)		1.002-1.030 g/ml (all)
Volume		0.8-2 L/d, average 1.1 L/d.
Ammonium (NH_4^+)	18.05	15-56 mmol/d (all)
Calcium (Ca^{2+})	40.08	Males: <250 mg/d
		Females: <200 mg/d (18-77)
Chloride (Cl^-)	35.45	40-224 mmol/d (all)
Citrate ($C_6H_5O_7^{3-}$)	192.12	221-1191 mg/d (20-40)
Creatinine ($C_4H_7N_3O$)	113.12	Males: 955-2936 mg/d
		Females: 601-1689 mg/d
Magnesium (Mg^{2+})	24.31	51-269 mg/d (18-83)
Oxalate ($C_2O_4^{2-}$)	88.02	0.11-0.46 mmol/d (all)
Phosphate (PO_4^{2-})	94.97	20-50 mmol/d (>18)
Potassium (K^+)	39.10	17-77 mmol/d (all)
Sodium (Na^+)	22.99	41-227 mmol/d (all)
Sulphate (SO_4^{2-})	96.06	7-47 mmol/d (all)
Urea (CH_4N_2O)	60.06	10-35 g/d (all)
Uric Acid ($C_5H_4N_4O_3$)	168.11	<750 mg/d (>16)

2.2 Artifical urine (AU)

Since human urine can be influenced by many factors, the artificial urine (AU) is prefered for research and educational purposes. For this reason, some AU protocols available in literature is presented below.

A commercial AU was invented by Laith Haddad and patented in USA [17]. Urea and creatinine were the organic substances on this AU formula. Urea constitutes ~95% of the nitrogen content of urine, and creatinine may be twice than uric acid in the urine. Also, the principle inorganic constituents evaluated in this AU are chlorides, phosphates,

sulphates and ammonia. Lock J *et al.* [14] used this information to evaluate the degradation of Mg alloys in AU for potential resorbable ureteral stent applications. This AU solution formulation is used in this project, so, the exact composition of AU formula is presented in the Chapter 3 on this work.

Sarigui *et al.* [18] presented, a multi-purpose artificial urine formulation which imitates a healthy human urine. Their formulation (MP-AU) is compared to other AU formulations in literature: formula for studying the growth of urinary pathogen by Brooks, T. and Keevil, W. (BK-AU) [19] and formula for *in vitro* cellular study by Chutipongtanate, S. and Thongboonkerd, V. (CT-AU) [20].

CT-AU fails to mimic the urine of health young people [18]. Meanwhile, BK-AU includes a not naturally component found in human urine, the bicarbonate [18]. Thus, MP-AU is the closest formulation to human urine [18].

2.3 Urinary tract obstruction

The urinary system is susceptible to variety diseases or conditions. They include urinary tract infection (UTI), kidney stones, and congenital anomalies which amongst another affect urinate.

Obstruction at any point in the urinary tract is another medical condition. Any complete or partial obstruction on the urological system can slow the flow of urine and increase the pressure in the tract. There are many causes of upper or lower urinary tract obstruction: congenital or acquired, stones anywhere in the urinary tract and health conditions. Some health problems can be: infections, cancer, gastrointestinal complaints, and ureteral obstructions [21, 22], (see Figure 3).

For instance, men, particularly those over 60, have obstruction in the urinary tract due to the prostate which tends to increase in size and block the flow of urine [23]. Patients with urinary obstruction had higher morbidity and mortality than patients without it [24].

Ureteral stent, urinary catheter, percutaneous nephrostomy[1], and nephrectomy[2] are some procedures to decompress the urinary tract [25]. Ureteral stents are considered effective (level of evidence 1b[3]) for decompression of the urology system by the European Association of Urology guidelines [26].

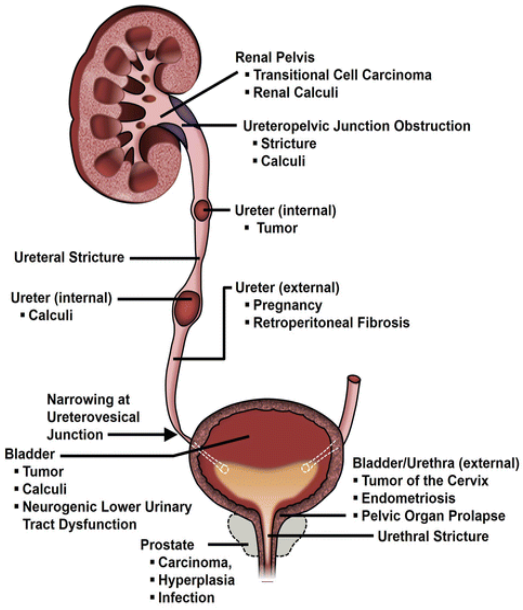

Figure 3. Upper and lower urinary tract causes and sites of obstruction *[22]*.

2.4 Ureteric stents

Ureteric stent, or ureteral stent, is a thin tube inserted into the ureter, placed for short- or long-term use. Ureteric stent is an indispensable common medical device used in the management of ureteric obstruction.

Ureteric stents facilitate the flow of urine from the kidney to the bladder in blocked ureters [14]. One clinical scenario where ureteric stent is used is in stone-forming patients, where the medical device avoids obstruction of the ureter and helps urinary function (see Figure 4) [5].

1 Percutaneous nephrostomy is an interventional procedure for decompression of the renal collecting system. This procedure involves inserting a catheter, through the skin, into the kidney to drain the urine into a collecting bag, outside the body [152].
2 Nephrectomy is a surgical procedure to remove all or part of a kidney [153].
3 According to Oxford Centre for Evidence-Based Medicine Levels of Evidence, level 1b is a prospective cohort study with good follow-up under a period of 1-6 months or 1-5 years to acute or chronic diagnosis, respectively [154].

Few years ago, ureteric stents have been investigated; however, an ideal stent without significant side effects is yet to be engineered. Generally, ureteric stents are associated with physical and psychologically problems and clinical complications, which influence patients' health-related quality of life. Some complications are, encrustation, bacterial adhesion, mispositioning, and stent fracture [14, 27]; such complications require a second procedure to take out the stent [5].

To reduce side-effects related to ureteral stents, evolution of several features and novel ureteral stent models with improved efficiency have been explored

2.4.1 Stents complications

After placement of ureteric stent in the urinary system, the creation of anchor points and biofilm success for the deposition of urine components around the surface of the stent. In the biofilm, the bacteria may adhere and start to grow, developing, at the end, the encrustation [5]. Figure 4 shows the previous conditions mentioned when the stent is inserted into the ureter.

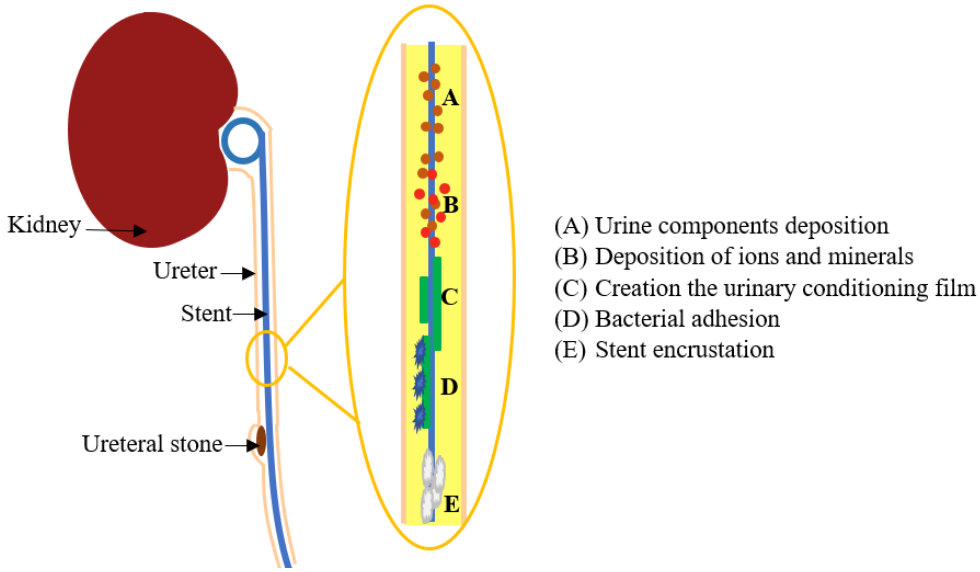

Figure 4. Conditioning film, bacterial adhesión and stent encrustation after placement of ureteric stent.

Bacterial colonisation, also, induces a simple urinary tract infection (UTI); however, if the UTIs are not controlled correctly, complicated UTIs usually affect structural or anatomic factors [28].

Other side-effects related to ureteral stents include that the stent might penetrate the ureter or kidney due to improper placement of it or ureteral peristalsis can cause stent migration [29]; occasionally, stents are forgotten and cause difficulties due to their splintering and disintegration, as well as stent fractures due to the harsh interaction between the urine and stent material.

Therefore, an appropriate stent length and avoiding coated stent with hydrophilic material should be selected to prevent mispositioning [27]. Stent position follow up can be done with computed tomography (CT), ultrasound [30] and X-ray [31]; however, to date, the best remedy to reduce any undesired consequence of stent is to remove it.

All complications relate with a stent are directly proportional to the time the device remains within the urinary tract [27]. Thus, biodegradable ureteral stents offer clinical benefits.

2.4.2 Engineering solutions

As stent is indispensable medical device in the area of urology, it should be redesigned to improve their tolerance reducing the unfavourable effects of the stent. Following, ideal ureteric stent, stent material principles and ureteric stent designs are described.

2.4.2.1 Ideal ureteric stent

The characteristics of an ideal ureteral stent [32, 33] should include: easy manoeuvrability, resistance to migration, biological inertia, resistance to fouling and infection, chemical stability in urine, radiopaque or visible with ultrasound, resistant to encrustation (calcification), excellent urine flow, and affordable.

In other words, an ideal ureteric stent should possess the following characteristics: biocompatibility, biodegradability, suitable mechanical properties and shape.

2.4.2.2 Stent material principles: biomaterial, biocompatible, biodegradable

Hudecki *et al.* [34] defined a biomaterial as “a substance that has been engineered to take form, which, alone or as a part of a complex system, is used to direct, by control of

interactions with components of living systems, the course of any therapeutic or diagnostic procedure".

Since biomaterials are in contact with the human body, these materials must be biocompatible. This means, that the biomaterial can be present in a physiological environment without adversely affecting the environment or the environment rejecting the material [35].

Although the presence of body fluids and friction between the implant and other tissues allow degradation of biomaterials, some biomaterials are destined to undergo degradation within the host's organism over a period, where the released breakdown product is biocompatible (biodegradable). The use of biodegradable materials in urological applications avoids the need to perform a second surgery to remove ureteral stents [32, 36].

2.5 Ureteric stent designs

Different shapes of ureteric stents have been developed through years (Figure 5).

- Open-ended ureteral stent: In 1967, Zimskind P.D *et al.* [37] used an indwelling silicone ureteral in the clinic. This stent is an open-ended, which has no coils and can provide temporary drainage [38], but produces reflux [37] (Figure 5(a)). Avoiding massive encrustation and migration, different designs of end segment-stent are developed, see Figure 5(b, f).

- Double pigtail (double-J) stent: To date, this shape is considered as the standard of the ureteric sten. The J shape in each end of the stent secures it in the kidney and the bladder, to prevent migration. This stent decreases urological complications such as and urinary tract irritation and infection [39], see Figure 5(c).

- Spiral or grooves stents: To improve urine flow through the ureter, the standard double-J was modified. New designs have spiral or grooves along the exterior of the stent [40], Figure 5(d, g) respectively.

- Tail stents: Another variation of double-J stents are tail stents. These are double J stents with an elongated closed-tip tail in the distal end to decrease stent-related bladder irritability and pain by less material in situ [41] , Figure 5(e); similar to tail stents are pigtail suture stent, which in the lower part has a 0.3 Fr[4] suture [42].

- Magnetic stent: magnetic material-tipped ureteral stent, Figure 5(h), used to eliminate the morbidity related to stent removal and reduce the clinical cost that require the standard double-J stents [43].

- Dual-durometer stents: Stents which incorporate a smooth transition of a biomaterial between at the renal end to the bladder [44], Figure 5(i).

Furthermore, the ureteral stent shape can be modified with variable stent lengths and diameters. An increase in the flow is correlated with an increase in the internal diameter of the ureteral stent. In contrast, stent's external diameter is not correlate with increase of extraluminal flow [45]. Symptoms worsen with too long stent, but too short stent can result in migration [46, 47].

Some investigations have been describing the relationship between ureteral stent size and stent-related symptoms (SRS). Up to now only Cubuk *et al.* [48] demonstrated that ureteral stent sizes, 4.8 Fr and 6 Fr, affect SRS; where 4.8 Fr ureteral stent improved SRS. Other studies compared symptoms with different stents size; however, those did not find statistical differences in symptoms between the groups [49, 50, 51, 52].

Finally, to compare different types of stent in research for SRS, the Ureteral Stent Symptom Questionnaire (USSQ) is used. It includes several stent-affected health domains in six sections (38 items): urinary symptoms, body pain, general health, work performance, sexual matters, and additional problems [53]. However, Lingeman *et al.* [54] suggested the use of USSQ for longer term comparisons in studies with presence or not of stents.

[4] French scale (Fr) is used for denoting the outside diameter of tubular instruments [155]. Outside diameter (mm) = Fr * 0.33.

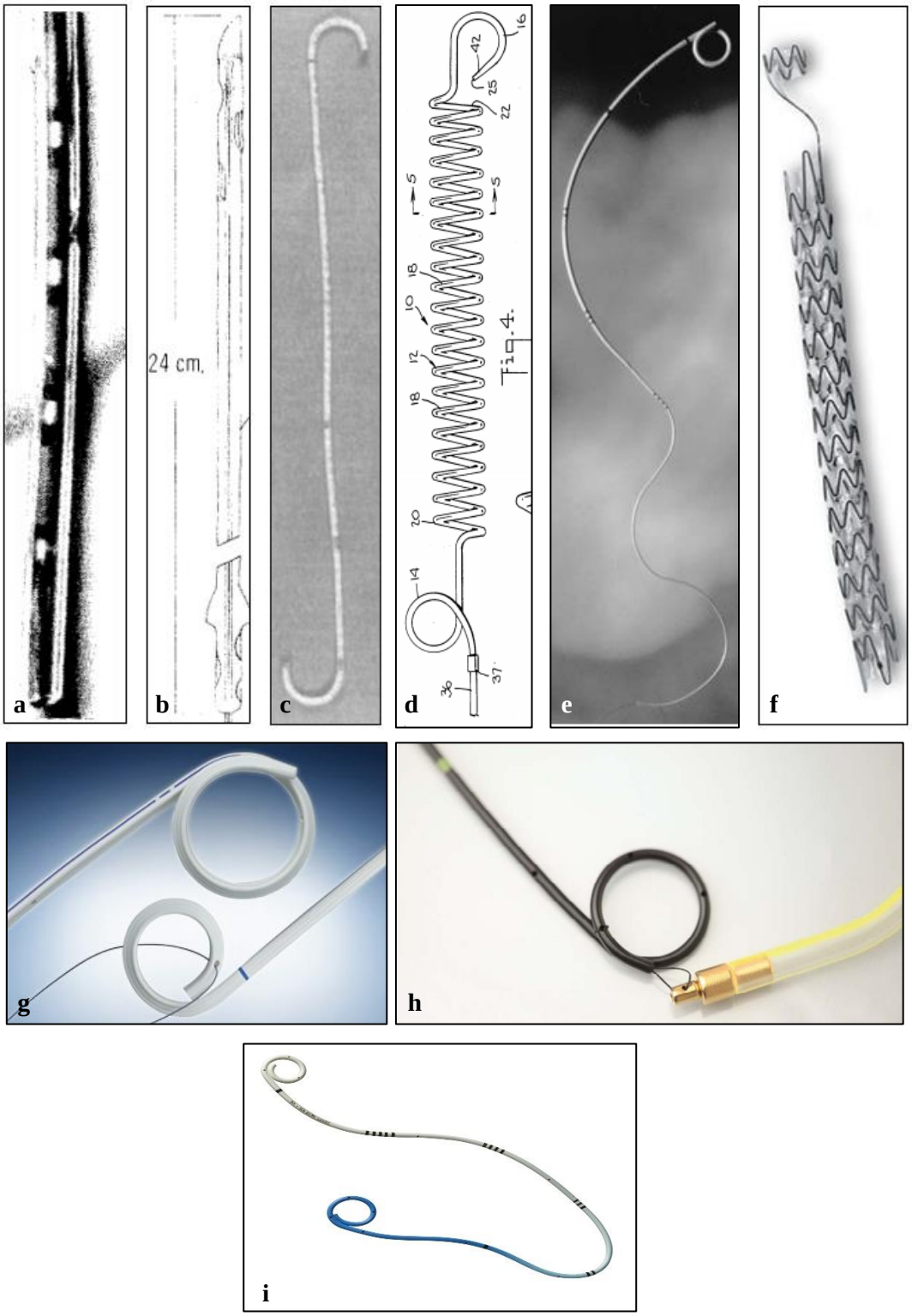

Figure 5. Stent architecture evolution through years.

(a)Open-ended silicone stent, 1967 [37]. (b)Silicone stent with a distal flange and sharply pointed barbs, 1974 [55]. (c)Silicone double J-stent, 1976 [56]. (d)Spiral stent, 1987 [57]. (e)Tail stent, 2002 [58]. (f)Self-expandable nitinol stent covered with a co-polymer. Model has an anchor segment to place in the renal pelvis or the bladder, 2012 [59]. (g)Olympus LithoStent™ ureteral stents. (h)Magnetic material tipped, 2017 [60]. (i)Stent ureteral PolarisTM Ultra, Boston Scientific.

2.6 Urological applications materials

Studies of materials for ureteral stents focus especially on biocompatibility, mechanical strength, flexibility and surface roughness.

Polymers and metals are the two main types of biocompatible materials that are generally used for fabricating ureteral stents.

2.6.1 Polymers

Different polymeric materials have been studied in urological applications. Silicone showed a less encrustation rate in artificial urine (AU) than polyurethane and Percuflex™ [5] [61]. However, restoration and maintenance of flow, difficulties during stent insertion, risk of stent migration are side effects related with silicone [35]. Percuflex™ was designed to obtain the shape of the ureter. Helical ureteral stent improves the behaviour of Percuflex™ [62].

Firm (polyurethane) and soft (Sof-flex[6]) stents showed significant differences in dysuria, kidney and suprapubic pain in the firm group [63]. Nevertheless, Joshi et. al. did not demonstrate difference in the quality of life of patients between ureteral stents composed of firm (Percuflex™) and soft polymer (Contour™ [7]) [64]. Another comparison is Polaris™ [8] ureteral stent with a soft tail versus Percuflex™ ureteral stent; which showed clinical advantages from Polaris™ over the conventional Percuflex™ [44].

Strength, versatility and low cost are the benefits of Polyurethane. Also, Polyurethane is ideal only for short term utilisation [35, 65], but generates epithelial ulcerations and erosion [66]. Polyether-urethane stents are associated with incrustation, infections, obstruction of the urinary tract for longer times (>3 months) and urologic stone formation [67].

---

[5] A proprietary olefinic block copolymer from Boston Scientific Corporation (Natick, MA, USA). Material name is not disclosed.

[6] A proprietary compound from Cook Urological (Spencer, IN, USA). Material name is not disclosed.

[7] Soft Percuflex™ stent with HydroPlus™ Coating from Boston Scientific Corporation (Natick, MA, USA). Material name is not disclosed.

[8] Dual durometer Percuflex™ stent with HydroPlus™ Coating featuring a distinct soft Nautilus™ Bladder Coil from Boston Scientific Corporation (Natick, MA, USA). Material name is not disclosed.

Other polymeric materials used in urological field include polypropylene and poly(ε-caprolactone) (PCL)/poly(lactide-co-glycolide) (PLGA). A polypropylene suture in pigtail suture stent was not calcificated 6 months after stenting [42]. And PCL/PLGA stent did not induce obstruction and had a control degradation in comparison to the polyurethane Shagong® stent [68].

2.6.1.1 Polymeric stent coatings

One approach to reduce encrustation, bacterial adhesion and complications in the placement of ureteral stents due to surface friction is to modify the surface of the ureteral stents. For this reason, various stent coatings have been explored.

Hydrogels are characterised for their lack of mechanical strength; however, strength is only important when it is used as a bulk material. As a coating it makes use of the strength of the substrate and at the same time reduce the friction coefficient and hence improving patient comfort especially since it also offers resistance to encrustation [69]. For this reason, C-Flex and Percuflex^{TM} are coated with hydrogels [35].

A hydrogel is defined as a wettable polymeric biomaterial able to swell in water but which does not dissolve in an aqueous environment [70]; characteristic of a hydrophilic material.

Hydrophilic coating ureteral stents need regular follow-up because they are encrusted *in vitro* [70], and did not reduce or prevent the bacterial adhesion [71].

Another alternative as biomaterial implanted in the urinary tract is Poly(vinyl pyrollidone)-coated polyurethane. It was more hydrophilic than either silicone or polyurethane; and avoid complications such as encrustation and bacterial adhesion [72].

The heparin-coated stent is used for long-term urinary drainage [73, 74]. Heparin is a glycosaminoglycan which is used as an anticoagulant and helps prevent cell adhesion [73]. Heparin coated stents were free of encrustation [74, 75, 76]; but, Lange D. *et al.* [77] showed that the bacterial adhesion in heparin-coated stent does not decrease.

Other stent coatings include either Pentosan Polysulfate, a semisynthetic polysaccharide considered as a low molecular weight heparin, useful in reducing the encrustation of long-term indwelling silicone stents in the human urinary tract [78]; and a diamond-like carbon coating effectively decreases friction, biofilm and encrustation formation [79].

2.6.2 Metals

Metals have better mechanical properties like strength and degradation properties compared to the polymeric material used in stent applications [80]. For this reason, commercial stents as, Allium Ureteral Stent (URS)[9], Memokath™ 051[10], Uventa™ [11], metal Resonance® ureteral stent[12] are available to use in clinical application. However, in recent years, some metal-based alloys have emerged as potential degradable biomaterials in the urinary field, to avoid removing the ureteral stent, and to decrease patient discomfort, encrustation and stent-related infection [81].

2.6.2.1 Permanent metals

Expandable titanium stent showed effective urinary flow re-establishment [82], and using nickel-titanium alloy (NiTinol) in urethral strictures' treatment is viable [83]. Moskovitz B. *et al.* [59] evaluated an ureteral stent made of a super-elastic nitinol and is covered with a new biocompatible, biostable polymer, the Allium URS. This stent prevents encrustation and it is used for temporarily long-term internal ureteral drainage. Another use of NiTinol is in the Memokath™ 051 stent, which is an alternative for non-curable ureteral obstruction [84], however migration and obstruction can occur [85].

Uventa™ stent has double-layered polytetrafluoroethylene membrane-covered self-expandable segmental NiTinol. This stent is an effective and safe option for palliative[13] treatment of intractable ureteral obstruction [86], with a higher clinical success rate than the Memokath™ 051 [87]. However, in long- term, the Uventa™ demonstrated complications with chronic ureteral obstructions and migration inconvenient [88].

The metal Resonance ureteral stent (made of a nickel–cobalt–chromium–molybdenum alloy) appears to have good tolerability [89] and effective for treating ureteric obstruction [30]; but, Liatsikos et al. [90] demonstrated that Resonance ureteral stent did not provide a significant reduction in encrustation rates.

[9] From Allium Medical Solutions (Israel).
[10] From PNN Medical (Denmark).
[11] From Taewoong Medical (Seoul, Korea).
[12] From Cook Medical (Bloomington, IN, USA).
[13] Specialized medical care focuses on providing to patient relief from the symptoms and stress of a serious illness [152].

2.6.2.2 Biodegradable ureteral stents (BUS)

BUS have emerged as a new generation of urological devices, reducing healthcare costs and risk to second removal of stent or the "forgotten stent syndrome". BUS, sometimes, are made of absorbable metal. The aim of the use of this kind of metal is that the corrosion products need to be non-toxic in a physiological environment.

For this reason magnesium (Mg) and its alloys are possible candidates for use in urological devices [14]; however, sometime show problematic degradation properties resulted in alkaline pH in the immersion solution due to hydrogen generation [14, 91], and the corrosion rate is too fast and the degradation behaviour is not homogeneous [92]. In contrast, mechanical properties of Fe-based alloys are appropriate, while the corrosion rate is low [93].

As a vascular stent and bone implant application, Zn has been studied as a relevant degradable metal with a moderate *in vitro* degradation rate compared to Fe and Mg. Then, Zn is the new target metal to be considered for stent applications in the urological field.

2.7 Zinc

Zn based alloys have been explored to overcome the limitations of magnesium and iron alloys. Fe and Mg have not shown a satisfactory combination of biocompatibility, controlled degradation rate and mechanical properties on *in vivo* and *in vitro* studies [94].

2.7.1 Toxicological aspects of Zn

In biological systems, Zn is recognised as a highly essential element for humans. Many biochemical processes involve Zn, for instance, in the regulation of repair mechanisms of DNA, in the cell cycle with the presence of transcriptional factors [95], signal messenger and neurotransmission [96], vitamin A metabolism [97], among others.

In the body, the distribution of Zn are: skeletal muscle[14] store about 60%, bones ~30%, and the liver and skin ~5%, the remaining percentage is located in the kidneys, brain, and pancreas [98]. So, zinc insufficiency or excess can moderate a cascade of

[14] Muscular system is conformed of skeletal, cardiac and smooth muscle.

metabolic processes that adversely affect the health of humans. Zinc excess can result from three major routes: inhalation, through the skin, or by ingestion [99], while zinc deficiency can be acquired or inherited.

Symptoms/consequences of Zn excess related with urological system are renal failure, mild albuminuria and red urine [100], in contrast, Zn deficiency effects are not described in the literature.

2.7.2 Mechanical properties of conventional and absorbable Zn-based alloys

Zn has an atomic number of 30, a molar mass of 65.38 g/mol, a density of 7.13 g/cm^3, and exhibits a single oxidation state (+2) [101]. Zinc is one of more used metal, including Fe, Al and Cu [102], with nearly 13 million tonnes produces around the world in 2018 [103]. In medical implants, the Zinc is used for bone regeneration [104] or repairing damaged blood vessels [80].

The common biomedical zinc alloys are shown in Table 2 and Table 3. Table 2 also displays the mechanical properties of zinc and its current alloys in biomedical applications, to use as references in this study.

Three studies, of pure Zn samples which recorded the micro-hardness test as shown in Table 2, will be described. Mostaed, E. *et al.* [93] used Zn cylindrical billets (99.995%) with a length and diameter of 60 mm and 15 mm, respectively. Vickers micro-hardness test was performed following ASTM E8-04 specification. The result is an average of five different measurements.

Sotoudeh, P. *et al.* [105] performed the Vickers microhardness measurement with a load of 100 g for 15 s and repeated 10 times. Using mechanical alloying powder process to their Zn samples. Finally, Tang, Z. *et al.* [106] used a 4N Zn wire (99.99+ wt%, Goodfellow Corporation, Oakdale, Pennsylvania). Vickers microhardness (HV) was measured using a load of 200 g for 5 s and repeated 18 times.

Table 2. Mechanical properties of pure Zn and Zn alloys. Adapted from [94].

Alloy (%wt)	Micro-hardness (HV)	YS (MPa)	UTS (MPa)	E (%)	Ref.
Zn[-]	34±1.7	51±3.7	111±4.5	60±5.9	[93]
Zn	-	45±3.5	61±3.7	3.8±0.8	[106]
Zn[-]	-	65	110	14	[107]
Zn	18	-	-	16	[105]
4N Zn	42±3	86±14	116±13	50±5	[108]
Zn-0.15Mg	52±4.9	114±7.7	250±9.2	22±4.0	[93]
Zn-0.02Mg[-]	-	136 ±2	167 ±4	27±3	[109]
Zn-0.02Mg[-D]	-	388±2	455 ±2	5.4±0.3	[109]
Zn-0.05Mg[-]	-	160	225	26	[107]
Zn-0.5Mg	65±3.9	159±8.5	297±6.5	13±0.9	[93]
Zn-0.5Mg	67±2	-	134 ±9	–4.8 ±0.7	[110]
Zn-0.8Mg	83±5	203±7	301±8	13.4±1.8	[111]
Zn-1Mg	75±3.9	180±7.3	340±15.6	6±1.1	[93]
Zn-1Mg[-]	65±10	90 ± 20	155±15	1.8±0.2	[112]
Zn-1Mg[-]	~ 78	-	-	-	[113]
Zn-1Mg	74±2	-	143 ±15	3.3 ±0.5	[110]
Zn-1Mg	-	-	120	0.4	[114]
Zn-1Mg	-	316	435	35	[114]
Zn-1Mg	65	-	153	1.5	[115]
Zn-1Mg	-	92	138	0.5	[116]
Zn-1Mg[-]	-	182	255	11.5	[116]
Zn-1Mg-0.5Ca[-]	~ 90	-	-	-	[113]
Zn-1Mg-1Ca	92 ±10	80 ±9	131 ±16	1±0.3	[117]
Zn-1Mg-1Ca[*]	-	205 ±10	257 ±13	5.2 ±1	[117]
Zn-1Mg-1Ca[**]	107 ±10	138 ±9	198 ±20	8.5 ±1.3	[117]
Zn-1Mg-0.1Mn	98	114	132	1.1	[118]
Zn-1Mg-0.1Mn[**]	108	195	299	26.1	[118]
Zn-1Mg-0.1Sr	94±7	109±14	132±10	1.4±0.4	[119]
Zn-1Mg-0.1Sr[**]	104±10	197±13	300±6	22.5±2.5	[119]
Zn-1Mg-0.5Sr	109±8	129±5	144±15	1.1±0.1	[119]
Zn-1Mg-1Sr	85±2	87±7	138±9	1.3±0.2	[117]
Zn-1Mg-1Sr[*]	-	202±5	253±18	7.4±1.3	[117]
Zn-1Mg-1Sr[**]	92 ±5	140 ±10	201 ±10	9.7 ±1	[117]
Zn-1.2Mg	93±7	117±1	130±6	1.4±0.6	[120]
Zn-1.2Mg[-]	967	220±15	363±5	21.3±2.3	[120]
Zn-1.5Mg[-]	100±10	-	150±25	0.5±0.3	[112]
Zn-1.5Mg	93	-	147	0.4	[115]
Zn-1.6Mg	97±4	232±8	368±8	4.4±0.3	[111]
Zn-2Mg	96±4	-	154 ±37	2.2 ±0.4	[110]
Zn-3Mg[-]	210±10	-	32±9	0.2±0.1	[112]
Zn-3Mg	117±6.1	291±9.3	399±14.4	1±0.1	[93]
Zn-3Mg	206	-	28	0.2	[115]
Zn-3Mg[*]	200±7	65±9	84±9	1.3±0.3	[121]
Zn-3Mg[hom]	175±8	36 ±3	46±1	2.1±0.1	[121]
Zn-3Mg[1-ECAP]	180±4	137±2	153±4	4.6±0.5	[121]
Zn-3Mg[2-ECAP]	186±4	205±4	220±3	6.3±0.9	[121]
Zn-5Mg	101±7	-	-	-	[110]
Zn-7Mg	106±2	-	-	-	[110]
Zn-0.5Al	59±5.8	119±2.3	203±9.6	33±1.2	[93]
Zn-1Al	73±4.6	134±5.8	223±4.3	24±4.2	[93]
Zn-4Al-1Cu	80	210	171	1	[112]
Zn-4Al-1Cu[-]	-	210	171	1	[112]
Zn–2Ag–1.8Au–0.2V[+]	61	129	231	59	[122]
Zn–2Ag–1.8Au–0.2V[+p]	96	168	233	17	[122]
Zn-2.5Ag[*]	-	147±7	203±5	35±4	[123]

(continued on next page)

Table 2 *(continued)*

Alloy (%wt)	Micro-hardness (HV)	YS (MPa)	UTS (MPa)	E (%)	Ref.
Zn-4Ag^{+}	73	157	261	37	[124]
Zn-4Ag^{+p}	82	149	215	24	[124]
Zn-5Ag*	-	210±10	252±7	37±3	[123]
Zn-7Ag*	-	236±12	287±13	32±2	[123]
Zn-1Cu	-	148.7±0.5	186.3±0.5	21.0±4.4	[106]
Zn–1Cu–0.1Ti	-	177	200	21	[125]
Zn–1Cu–0.1Ti*	72.6±0.6	86.1±2.6	92.4±4.4	1.4±0.8	[126]
Zn–1Cu–0.1Ti^{h**}	70.6±1.8	175.4±3.8	205.7±5.5	39.2±1.4	[126]
Zn–1Cu–0.1Ti^{hc**}	56.4±0.8	204.2±4.3	249.9±3.8	75.2±1.9	[126]
Zn–1.0Cu–0.2Mn–0.1Ti	-	196	212	19	[125]
Zn-2Cu	-	199.7±4.2	240.0±1.4	46.8±1.4	[106]
Zn-3Cu	-	213.7±1.2	257.0±0.81	47.2±1.0	[106]
Zn-3Cu*	367±1	247±8	288±4	45.9±3.	[127]
Zn-3Cu-0.5Fe*	761	232±3	284±2	32.7±4.2	[127]
Zn-3Cu-1Fe*	82±1	222±6	272±7	19.6±1.4	[127]
Zn-3Cu-0.1Mg*	-	340±15	360 ±15	5±1	[128]
Zn-3Cu-0.5Mg*	-	400±10	420±5	2±1	[128]
Zn-3Cu-1Mg	-	425±5	440 ±5	1±0.5	[128]
Zn-4Cu	-	250±10	270±10	51±2%	[129]
Zn-4Cu	-	227.0±5.0	270.7±0.5	50.6±2.8	[106]
Zn-4Cu*	-	250±10	270±10	51±2	[130]
Zn-1Ca-1Sr	91 ±12	86 ±5	140 ±9	1.2 ±0.2	[117]
Zn-1Ca-1Sr*	-	212 ±15	260 ±15	6.7 ±1.1	[117]
Zn-1Ca-1Sr**	87 ±7	144 ±9	203 ±10	8.8 ±1.2	[117]
Zn-0.2Mn^{-}	-	132	220	48	[131]
Zn-0.35Mn-0.41Cu	-	77	84	0.3±0.1	[132]
Zn-0.35Mn-0.41Cu**	-	198±7	292±3	29.6±3.8	[132]
Zn-0.4Mn^{-}	-	123	198	54	[131]
Zn-0.6Mn^{-}	-	118	182	71	[131]
Zn-0.75Mn-0.40Cu	-	113	120 ±3	0.4±0.1	[132]
Zn-0.75Mn-0.40Cu**	-	196±11	278±4	15.3±3.9	[132]
Zn–1Mn–0.1Ti	-	180	198	7	[125]
Zn-4Mn	102	-	-	14.9	[105]
Zn-24Mn	71	-	-	19.4	[105]
Zn-0.2Li**	98±6	240±10	360±15	14.2±2.0	[133]
Zn-0.4Li**	115±7	425±15	440±5	13.8±2.9	[133]
Zn-0.7Li**	137±8	475±50	565±2	2.4±0.4	[133]
Zn-0.8Li	-	183.5	238.1	75.0	[104]
Zn-0.8Li-0.2Mg	-	253.7	341.3	30.6	[104]
Zn-0.8Li-0.2Ag	-	196.2	254.7	97.9	[104]
Zn-Li^{-D}	97±2	238±60	274±61	17±7	[108]

*As cast; **rolled; ^{h**} hot rolled; ^{hc**} hot rolled plus cold rolled; $^{+}$thermomechanical treatment; $^{+p}$thermomechanical treatment additional precipitation hardening; ^{ECAP} equal channel angular pressing; $^{-}$extruded; $^{-D}$ extruded drawn; hom homogenized.

2.7.3 Corrosion behaviour and biodegradability of Zn-based alloys

Generally, cathodic and anodic reactions occur in the degradation of biodegradable metals in neutral physiological condition. In an aqueous solution, the corrosion form and the rate of zinc corrosion can be affected by pH, temperature, concentration and dissolved species [134].

Anions present in solution greatly affect the corrosion of zinc. Chloride and sulphate increase the solubility of zinc. In contrast, carbonate and phosphate reduce the solubility of zinc and promote the protective behaviour due to precipitation of zinc salts. Chromate reacts with the zinc surfaces and, depending on the reaction products, may form a passive film [134].

Eqs. (1)-(3) give the corrosion reactions of Zn [134] in aqueous solution. The anodic reaction, Eq. (1) shows the oxidation of Zn when exposed to body fluid. The corrosion products $Zn(OH)_2$ and ZnO form on the metal surface, where hydrogen gas release does not take place, according to Eqs. (2) and (3).

Anodic reaction: $Zn \rightarrow Zn^{2+} + 2e^-$ Eq. (1)

$Zn(OH)_2$ formation: $Zn^{2+} + 2H_2O \rightarrow 2Zn(OH)_2 + 2H^+$ Eq. (2)

ZnO formation: $Zn(OH)_2 \rightarrow ZnO + H_2O$ Eq. (3)

The dissolution of the corrosion products of Zn ($Zn(OH)_2$ and ZnO) in the surface promotes further corrosion of the exposed metal into soluble salts. If the physiological environment has high concentration of Cl^- ions, the formation of degradation products tends to break, generating pitting corrosion [134]. Moreover, in the pure Zn and Zn-based alloys, carbonate and phosphate ions have been found on the degradation products [135].

The pH value of the aqueous solution is another relevant aspect to consider in the degradation of Zn. According to Pourbaix diagram (Figure 6) over the pH range of 0-9 and the potentials ~820 mV to ~ −670 mV, Zn is present as hydrated Zn^{2+} (aq). But, in the pH range of 7–10, protective layer is not formed due to the lower cathodic reaction rates [134]. Thus, over time, the Zn samples immersed in a solution of pH of ~7.4 will dissolve.

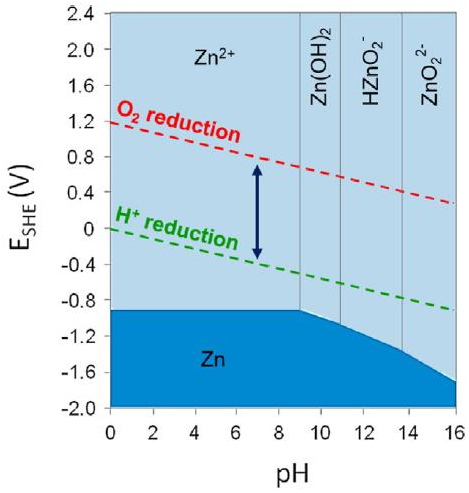

Figure 6. Pourbaix diagram of Zn [94].

Table 3 provides summaries information obtained from corrosion studies of Zn and Zn-based alloys for biomedical purposes where only one study was done with artificial urine (AU), highlighted in blue.

Champagne *et al.* [136] studied the *in vitro* degradation behaviour of absorbable zinc alloys in artificial urine (AU). In this study the corrosion rate varies under all the alloys evaluated (pure Zn, Zn-0.5 Al and Zn-Mg) with pure Zn having the lowest value. Also, hydroxide, carbonate, phosphate, and oxygen are the compounds of the corrosion layer in the Zn group. They conclude that the Zn-0.5Al has a uniform corrosion layer due to the low affinity with the ionic compounds in the AU [136].

Meanwhile, an *in vitro* study evaluated the bioabsobable behaviour of pure Zn and Zn-Mg alloy in rat bladder. Okamura, Y. *et al*. [137] observed the time-dependent volume reductions in urine. In this study, Zn-1.8Mg has a better degradation than pure Zn.

Table 3. Degradation rates of different Zn and Zn-based alloys form immersion (CRI) and electrochemical (CRE) tests. Adapted from [94].

Alloy (%wt)	Solution	pH	OCP (V)	CRE (mm/year)	CRI (mm/year)	Ref.
Zn–0.8Mg	-	-	-	0.0134±0.0003	-	[111]
Zn	AU	6.00	-1.11±0.06	0.87±0.09	-	[136]
Zn-0.5Mg	AU	6.00	-1.18±0.01	1.39±0.07	-	[136]
Zn-1Mg	AU	6.00	-1.17±0.01	1.50±0.08	-	[136]
Zn-0.5Al	AU	6.00	-1.15±0.01	1.14±0.03	-	[136]
Zn*	c-SBF	-	-	-	0.022±0.005	[106]
Zn-1Cu*	c-SBF	-	-	-	0.033±0.001	[106]
Zn-2Cu*	c-SBF	-	-	-	0.027±0.005	[106]
Zn-3Cu*	c-SBF	-	-	-	0.030±0.004	[106]
Zn-4Cu*	c-SBF	-	-	-	0.025±0.005	[106]
Zn	DMEM	-	-	-	6.85±0.02	[124]
Zn-4Ag+	DMEM	-	-	-	10.75±0.16	[124]
Zn–1Cu–0.2Mn–0.1Ti	FeSSIF	5.00	-	-	0.12	[125]
Zn–1Cu–0.1Ti	FeSSIF	5.00	-	-	0.13	[125]
Zn–1Mn–0.1Ti	FeSSIF	5.00	-	-	0.11	[125]
Zn	Hank	7.40	-	0.137±0.004	-	[93]
Zn-	Hank	7.40	-	0.134±0.008	0.074±0.004	[93]
Zn*	Hank	7.40	-	0.157±0.012	-	[138]
Zn h**	Hank	7.40	-	0.306±0.019	-	[138]
Zn	Hank	-	-0.992	0.036±0.007	0.023±0.006	[139]
Zn	Hank	-	-	0.05±0.01	-	[119]
Zn-	Hank	7.40	-	0.133±0.010	0.077±0.004	[123]
Zn	Hank	-	-	2.71	-	[105]
Zn-0.5Al*	Hank	7.40	-	0.165±0.009	-	[93]
Zn-0.5Al-	Hank	7.40	-	0.143±0.008	0.079±0.005	[93]
Zn-1Al*	Hank	7.40	-	0.166±0.007	-	[93]
Zn-1Al-	Hank	7.40	-	0.145±0.007	0.078±0.006	[93]
Zn-2.5Ag-	Hank	7.40	-	0.137±0.021	0.079±0.007	[123]
Zn-5Ag-	Hank	7.40	-	0.144±0.007	0.081±0.001	[123]
Zn-7Ag-	Hank	7.40	-	0.147±0.018	0.084±0.005	[123]
Zn-0.5Ca	Hank	-	-1.031,	0.042±0.013	0.035±0.005	[139]
Zn-1Ca	Hank	-	-1.033,	0.057±0.009	0.040±0.003	[139]
Zn-1Ca-1Sr	Hank	-	-	0.19±0.01	0.11±0.01	
Zn-2Ca	Hank	-	-1.044	0.084±0.021	0.074±0.010	[139]
Zn-3Ca	Hank	-	-1.041	0.062±0.017	0.066±0.003	[139]
Zn–1Cu–0.1Ti	Hank	5.42	-	-	0.02	[125]
Zn–1Cu–0.1Ti*	Hank	7.40	-	0.315±0.006	-	[126]
Zn–1Cu–0.1Ti h**	Hank	7.40	-	1.628±0.013	-	[126]
Zn–1Cu–0.1Ti hc**	Hank	7.40	-	0.991±0.007	-	[126]
Zn–1Cu–0.2Mn–0.1Ti	Hank	5.42	-	-	0.02	[125]
Zn-3Cu*	Hank	-	-	0.005	0.012±0.003	[128]
Zn-3Cu-0.1Mg*	Hank	-	-	0.018	0.023±0.002	[128]
Zn-3Cu-0.5Mg*	Hank	-	-	0.024	0.030±0.003	[128]
Zn-3Cu-1Mg*	Hank	-	-	0.180	0.043±0.004	[128]
Zn-4Cu h-	Hank	-	-	0.009±0.001	-	[129]
Zn-0.15Mg*	Hank	7.40	-	0.172±0.003	-	[93]
Zn-0.15Mg-	Hank	7.40	-	0.164±0.003	0.079±0.004	[93]

(continued on next page)

Table 3 *(continued)*

Alloy (%wt)	Solution	pH	OCP (V)	CRE (mm/year)	CRI (mm/year)	Ref.
Zn-0.5Mg[-]	Hank	7.40	-	0.164±0.008	0.081±0.002	[93]
Zn-0.5Mg[*]	Hank	7.40	-	0.175±0.004	-	[93]
Zn-1Mg[-]	Hank	7.40	-	0.169±0.006	0.083±0.004	[93]
Zn-1Mg[*]	Hank	7.40	-	0.177±0.007	-	[93]
Zn-1Mg-0.1Mn	Hank	7.40	-	0.26	0.12	[118]
Zn-1Mg-0.1Mn[**]	Hank	7.40	-	0.25	0.11	[118]
Zn-1Mg-0.1Sr	Hank	-	-	0.12±0.01	-	[119]
Zn-1Mg-0.1Sr[**]	Hank	-	-	0.15±0.05	-	[119]
Zn-1Mg-0.5Sr	Hank	-	-	0.11±0.01	-	[119]
Zn-1.2Mg	Hank	-	-	0.12	0.08±0.01(30 d) 0.07±0.01(90 d)	[120]
Zn-1.2Mg[-]	Hank	-	-	0.19	0.11(30 d) 0.09±0.02(90 d)	[120]
Zn-1.5Mg-0.1Mn	Hank	7.40	-	0.14	0.09	[118]
Zn-3Mg[-]	Hank	7.40	-	0.128±0.005	0.076±0.005	[93]
Zn-3Mg[*]	Hank	7.40	-	0.135±0.006	-	[93]
Zn-4Mn	Hank	-	-	0.72	-	[105]
Zn-24Mn	Hank	-	-	0.02	-	[105]
Zn-5Ge[*]	Hank	7.40	-	0.1272±0.0132	-	[138]
Zn-5Ge [h**]	Hank	7.40	-	0.2255±0.0146	-	[138]
Zinc	Human plasma	-	-1.09 to -1.11	0.3±0.1	-	[135]
Zn-4Ag[+]	McCoy's 5A	-	-	-	0.00380±0.0014	[124]
Zn	McCoy's 5A	-	-	-	0.00289±0.0008	[124]
Zn	PBS	-	-	-	0.0087±0.0035	[122]
Zn	PBS	7.40	-1.00	<0.1	-	[135]
Zn-1Mg[-]	PBS	7.40	-	0.012±0.002	-	[113]
Zn-1Mg-0.5Ca[-]	PBS	7.40	-	0.066±0.004	-	[113]
Zn–Ag–Au–V[+]	PBS	-	-	-	0.007±0.006	[122]
Zinc	Ringer	7.40	-1.06	0.15 to 0.3	-	[135]
Zn-0.8Li	Ringer	7.40	-	0.12	-	[104]
Zn-0.8Li-0.2Mg	Ringer	7.40	-	0.17	-	[104]
Zn-0.8Li-0.2Ag	Ringer	7.40	-	0.11	-	[104]
Zn	SBF	-	-	0.0050 to 0.0075	-	[135]
Zn	SBF	7.40	-	0.653	0.15	[107]
Zn	SBF	7.20 to 7.40	-	0.16	-	[133]
Zn-0.5Al	SBF	-	-	0.0204±0.0013	-	[110]
Zn-0.5Al-0.5Mg	SBF	-	-	0.0095±0.0003	-	[110]
Zn-3Cu[*]	SBF	-	-	0.085	0.045±0.008	[127]
Zn-3Cu-0.5Fe[*]	SBF	-	-	0.105	0.064±0.004	[127]
Zn-3Cu-1Fe[*]	SBF	-	-	0.130	0.069±0.007	[127]
Zn-0.2Li[**]	SBF	7.20 to 7.40	-	0.06	-	[133]

(continued on next page)

Table 3 *(continued)*

Alloy (%wt)	Solution	pH	OCP (V)	CRE (mm/year)	CRI (mm/year)	Ref.
Zn-0.4Li[**]	SBF	7.20 to 7.40	-	0.05	-	[133]
Zn-0.05Mg[-]	SBF	7.40	-	0.728	0.15	[107]
Zn-Mg	SBF	-	-	0.0050–0.0075	-	[135]
Zn-1Mg[-]	SBF	-	-	0.08	0.070	[112]
Zn-1Mg	SBF	6.50	-	0.053	-	[115]
Zn–1Mg[*]	SBF	-	-	-	0.28±0.01	[116]
Zn–1Mg[-]	SBF	-	-	-	0.12±0.05	[116]
Zn-1.5Mg	SBF	6.50	-	0.058	-	[115]
Zn-1.5Mg[-]	SBF	-	-	0.08	0.063	[112]
Zn-3Mg	SBF	6.50	-	0.052	-	[115]
Zn-3Mg[-]	SBF	-	-	0.08	0.070	[112]
Zn-3Mg[hom]	SBF	7.40	-	0.30	0.25	[121]
Zn-3Mg[hom 1-ECAP]	SBF	7.40	-	0.24	0.18	[121]
Zn-3Mg[hom 2-ECAP]	SBF	7.40	-	0.28	0.19	[121]
Zn-0.35Mn-0.41Cu	SBF	7.40	-	-	0.050±0.004	[132]
Zn-0.75Mn-0.40Cu	SBF	7.40	-	-	0.065±0.006	[132]
Zinc	Whole blood	-	-1.12	0.05 to 0.2	-	[135]

[*]As cast; [**]rolled; [h**] hot rolled; [hc**] hot rolled plus cold rolled; [+]thermomechanical treatment; [+P]thermomechanical treatment additional precipitation hardening; [ECAP] equal channel angular pressing; [-]extruded; [-D] extruded drawn; hom homogenized; FeSSIF Fed-state simulated intestinal fluid.

2.8 Techniques for electrochemical degradation

Engineers and scientists use different experimental procedures to study the chemical and metallurgical characteristic for each material, prior insertion of it in the human body. Identifying also side-effects with degradation of biomaterials. In aqueous solution, transfer of electronic charge is involved in all metallic corrosion processes. Therefore, the electrochemical nature of corrosion is studied.

Electrochemical polarisation methods include potentiostatic techniques where the potential is controlled. Potentiostatic techniques are: open circuit potential (OCP), potentiodynamic polarisation (PDP), electrochemical impedance spectroscopy (EIS), scanning vibrating electrode technique (SVET) and scanning electrochemical microscope (SCEM).

2.8.1 Open circuit potential (OCP)

The electrochemical corrosion potential, also known as OCP, uses a metal immersed in aqueous environment and a standard reference electrode (SRE) to obtain voltage

difference between them. Transitions between passive and active states and the time needed for the system to reach a constant state can be provided for the OCP [140].

2.8.2 Potentiodynamic polarisation (PDP)

The technique PDP implies a variation of the potential of the electrode over a large range at a selected rate, while through the electrolyte flows the current [140]. PDP provides information on the degradation rate of materials. A PDP sweeps the potential between two set values to cover the anodic and cathodic branch [141].

Two methods are available for measurement of corrosion by electrochemical polarisation, a Tafel extrapolation and polarisation resistance. Only Tafel extrapolation was used in this project, for this reason is described below.

2.8.2.1 Tafel extrapolation

To determine the corrosion current density T, i_{corr} (mA cm^{-2}), and thus, determine the corrosion rate, Tafel extrapolation of polarisation curves is used. Extrapolation of the linear portion of the curve to corrosion potential (E_{corr}), both anodic and cathodic branch, is utilized to gain the corrosion current density, as depicted in Figure 7.

However, the formation of thin films on certain metallic surfaces under oxidising conditions may generate corrosion resistance on the samples [141]. This condition is known as passivity.

The passive behaviour displays the polarisation curve as shown in Figure 8. The parameters displayed are based on empirical observation [142]. Some studies identified passive behaviour on Zn samples, as the present study.

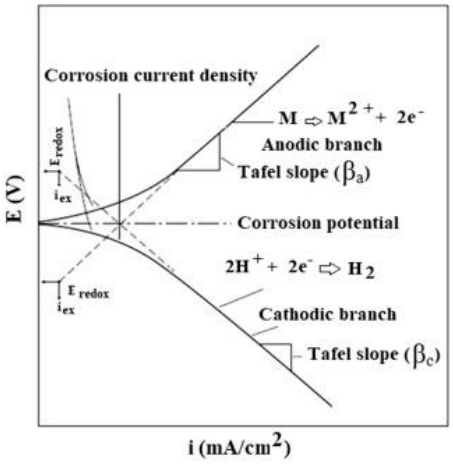

Figure 7. Example of Tafel extrapolation, corrosion of metal in acidic aqueous medium [143].

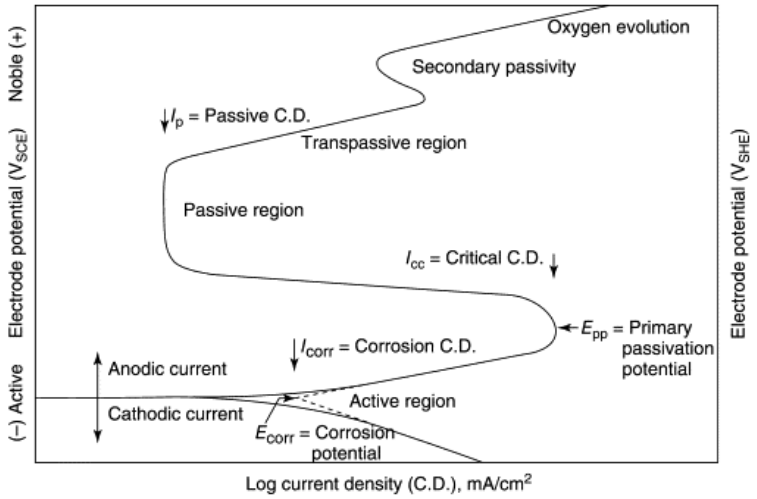

Figure 8. Hypothetical cathodic and anodic polarisation plot for determining localized corrosion parameters [142].

Chapter 3

Materials and Methods

3.1 Material specification and characterisation

Pure zinc, sheet and wire, samples used throughout this work were supplied by Advent Research Materials (UK). Pure Zn sheet samples were 3.0 mm thick, sized 50 mm x 50 mm and was specified to be of 99.9% purity. Pure Zn wire sample had 1.0 mm diameter and were specified to be of 99.99% purity.

Characterisation of both Zn samples was carried out by scanning electron microscopy (SEM), energy dispersive spectroscopy (EDS) and X-ray diffraction (XRD).

The crystalline phases of both Zn samples were investigated, prior tests, using a Bruker D8 Advance X-Ray diffractometer (Germany), with a Bragg-Brentano setup. The diffractometer made use of a copper tube X-ray target and a Cu-Kα radiation ($\lambda = 0.154$ nm). The Zn sheet sample analysed was cut to a 15 x 15 mm square and the Zn wire sample was cut into pieces of 12 mm each to cover an area of about 12 x 12 mm.

The scanning range was $2\theta = 20° - 90°$, scanning step was of 0.02° at a dwell time of 0.5 s; with a voltage and current of 45 kV and 40 mA, respectively. The diffraction patterns obtained were analysed and indexed using X'Pert High Score analytical software.

A Zeiss Merlin Field Emission scanning electron microscope (Germany), was used with current and voltage setting at 15 kV and 225 nA, respectively. SEM was used to verify the surface of wire samples prior immersion test. Also, EDS analysis was carried out to analyse the chemical composition in (wt.%) of elements presents in the surface of the Zn samples prior tests. In this characterisation method the Zeiss SEM was equipped with an Apollo X Ametek EDS detector (USA).

3.2 AU solution preparation

To evaluate the corrosion resistance of Zn-based samples, the artificial urine was used as the corrosion solution. The AU solution was used without further purification. All chemicals used in this study were in powder form. For a practical and economical AU formulation, the composition of the AU solution was based on U.S. patent #7109035 [17], see table 4; and the AU solution preparation published by Lock J *et al.* [14].

Table 4. AU solution composition brought to 500 ml by adding distilled H_2O (diH_2O) and tris solution.

Component		Mass (g)
Ammonium Phosphate dibasic*	$(NH_4)_2HPO_4$	0.85
Calcium Chloride+	$CaCl_2$	0.12
Creatinine*	$C_4H_7N_3O$	0.75
Magnesium chloride hexahydrate*	$Cl_2Mg \cdot 6H_2O$	0.25
Potassium chloride-	KCl	1.01
Sodium Sulphate*	Na_2SO_4	1.01
Urea*	CH_4N_2O	0.38

Suppliers: *BIOCHEM Chemopharma, France. +Levo Laboratory Service, Malta. -Avonchem Ltd, UK.

The chemicals were weighed with the precision balance Kern PLJ (Balingen, Germany) and were crushed in the order provided in Table 4 and dissolved in a Tris solution. Since Zinc corrosion can be affected for the pH of the aqueous solution, tris solution in the AU was used to maintain a stable pH.

A tris solution was prepared with 6.06 g Tris(hydroxymethyl)aminomethane (BIOCHEM Chemopharma, France) diluted with 60 ml diH_2O. Then, 4.60 ml HCl (BIOCHEM Chemopharma, France) was added and, finally, the solution was diluted to 100 ml with diH_2O. Then, the solution was diluted with diH_2O to create 500 mL of AU solution with a stabilised pH around 7.

The AU solution was stirred with a magnetic stirrer at 320 rpm. Also, the temperature of the solution is kept constant at 37 ± 0.5°C using the heater function of the stirrer (VWR Hotplate/Stirrer MET 355).

Figure 9 is a summary of the schematic description of the AU solution preparation process. After the preparation of AU, Universal Indicator Paper pH 1-14 (Metria CSPH 002 001) was used for pH verification. The AU solution was stored at 4°C. Since the pH

was taken into account in the corrosion properties tests of the Zn based samples, the AU solution used was prepared at most one day prior to the research study [18].

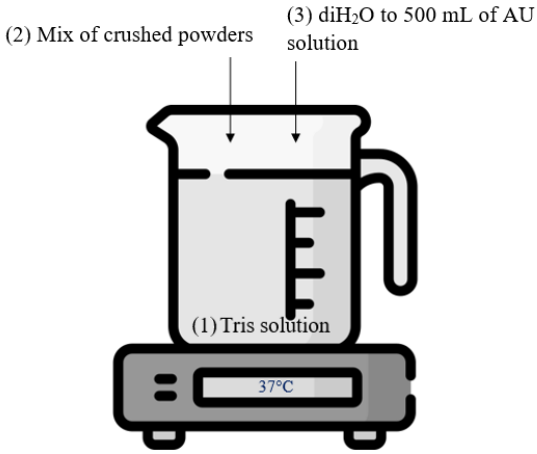

Figure 9. Schematic of the AU solution preparation.

3.3 Vickers microhardness test

The mechanical Vickers microhardness test was carried out to characterise the mechanical properties of the Zn samples. The zinc wire sample as received was mounted in a cold mounting resin coupon Tri-Hard Cold Mounting Resin supplied by MetPrep Ltd. (UK). The resin coupon was 30 mm diameter.

Coupon was ground using silicon carbide paper starting from grit size P2500 up to grit size P4000 to achieve a flat surface and remove any oxide layer. Sample was then polished using a 1µm diamond suspension on a Kemet polishing pad.

Vickers microhardness (HV) was measured using a Mitutoyo MVK-H2 (Tokyo, Japan) micro-hardness testing machine with a Vickers hardness indentor. Indentations were made on the surface at a load of 50gf. Measurements were repeated ten times.

3.4 Corrosion testing

3.4.1 *In vitro* degradation testing, Zn sheet samples

3.4.1.1 Electrochemical corrosion test

Two methods of electrochemical corrosion test were conducted: open circuit potential (OCP), and potentiodynamic polarisation (PDP).

All samples were ground with silicon carbide abrasive paper from grit size P320, up to grit size P2400, then, for 15 minutes, the samples were immersed in ultrasonic bath with ethanol to remove surface particles, finally, the samples were rinsed with distilled water for 2 min, prior to electrochemical testing. The specimens were weighed after drying and test.

The specimen working area, 0.196 cm^2 (0.5 cm of diameter), was exposed to 300 mL of artificial urine (AU) solution and a solution temperature of 37 ± 1 ºC was maintained for the duration of the OCP and PDP tests. Four repeats were performed to obtain statistical conclusions.

OCP and PDP were performed one after another on all metal specimens in accordance with the ASTM G59: *Standard Test Method for Conducting Potentiodynamic Polarization Resistance Measurements.* A three-electrode cell configuration was used, the working electrode was the metallic samples, the counter electrode was a platinised titanium rod, and the reference electrode was a saturated calomel electrode (SCE). The electrodes were connected to a Gamry Interface 1000 potentiostat, (USA).

The OCP experiments were conducted for 3600 s and was followed by a PDP experiment using a scan rate of 0.167 mV/s, from -0.25 to +0.35 V (V vs OCP).

The corrosion rate (CRE) was calculated according to ASTM G102-89: *Standard Practice for Calculation of Corrosion Rates and Related Information from Electrochemical Measurements* using Eq. (4).

$$CRE = 3.27 \cdot 10^{-3} \frac{i_{corr} EW}{\rho} \qquad \text{Eq. (4)}$$

where CRE is the corrosion rate (mm $year^{-1}$), i_{corr} is the corrosion current density (µA cm^{-2}) deduced from Tafel extrapolation, EW is the equivalent weight of metal (32.68 g/eq for pure Zn [144]) and ρ is the density (7.13 g cm^{-3} for pure Zn).

Then, the tested samples were rinsed in an ultrasonication bath with ethanol. Subsequently, SEM was conducted in order to observe and characterise the degradation products on the surface. Also, EDS analysis was carried out to analyse the chemical composition in (wt.%) of elements presents on the surface of the Zn samples.

3.4.2 *In vitro* degradation testing, Zn wire samples

3.4.2.1 Set-up *in vitro* degradation for Zn wire samples

An apparatus to simulate the ureter of the human was designed and built to evaluate the corrosion resistance of the Zn wire. In the design, considerations were given to dimension of a ureter, which was based on adult men who did not have any diseases in their urinary system; the flow rate, temperature and the low pressure of transporting urine between kidney and urethra.

Considering the normal range volume of the urine as 0.8-2 L/d (0.55-1.38 mL/min), and that the rate of production of urine by the kidneys is equal to the mean rate of flow of urine through the ureter over a long period [145]. Hence, the ideal flow rate in the ureter is 0.55-1.38 mL/min; an average of 0.97 mL/min. Human urine also comes out of the body at 37ºC.

Moreover the ureter model used in this study was based on the data collected from Kyung-Wuk Kim et al. [11] where 19 healthy men patients, had three ureter models: tubular ureter, funnel-shaped and undulated ureter. Tubular ureter was selected, since the luminal flow rate was relatively constant along the whole ureter. According to this study, the length and the diameter of the ureter model was 226.21 mm and 4.57 mm, respectively.

Thus, Table 5 summarises the design criteria considered for the construction of the simulation apparatus. With these design criteria, a schematic set-up was elaborated (Figure 10). Which includes a peristaltic pump, a heater with negative feedback and a container of AU.

Table 5. Design criteria for set-up for *in vitro* degradation for Zn wire samples.

Design criteria	Value
Length of ureter	226.21 mm
Diameter of ureter	4.57 mm
Flow rate through ureter	0.97 mL/min
Temperature of urine	37ºC

The validation of this set-up car was carried out measuring each criteria triplicate for statistical analysis. The flow rate and temperature were identified every 2 hours while the peristaltic pump worked 6 hours continuously.

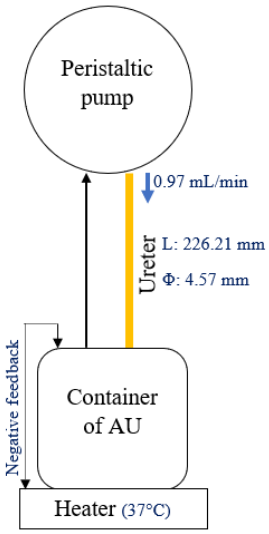

Figure 10. Schematic illustration of the *in vitro* degradation set-up used to investigate the degradation behaviour of zinc wire samples.

The apparatus created to evaluate the corrosion resistance of the Zn wire samples is shown in Figure 11(a). The ureter had 22.62 ± 0.02 cm length and 0.46 ± 0.02 cm diameter, avoiding undulations between the tract. The flow rate obtained, through the simulate ureter without Zn wire sample, was 1.01 ± 0.19 ml/min.

The set-up had a feedback of urine to avoid: (1) waste artificial urine solution and (2) because with trials, the pH of the AU solution not showed a change in contact with the samples over 7 h due to the use of tris buffer.

The assembly was made with a commercial peristaltic pump (12 V and 0.26 A), silicone pipe, 3-connector plastic (Y), air valves and non-return valves. Also, a big bowl covered with aluminium foil was used to control the temperature of the AU solution with heat transfer by hot conduction. The temperature was measured with a thermometer.

The position of the Zn samples is shown in Figure 11(b). The air valve was separated from the proximal end of the ureter to put or remove the zinc wire sample. The proximal end was used as the unique zone to touch directly the zinc wire samples. The silicone stopper avoided migration of the wire sample to the AU container (simulated bladder).

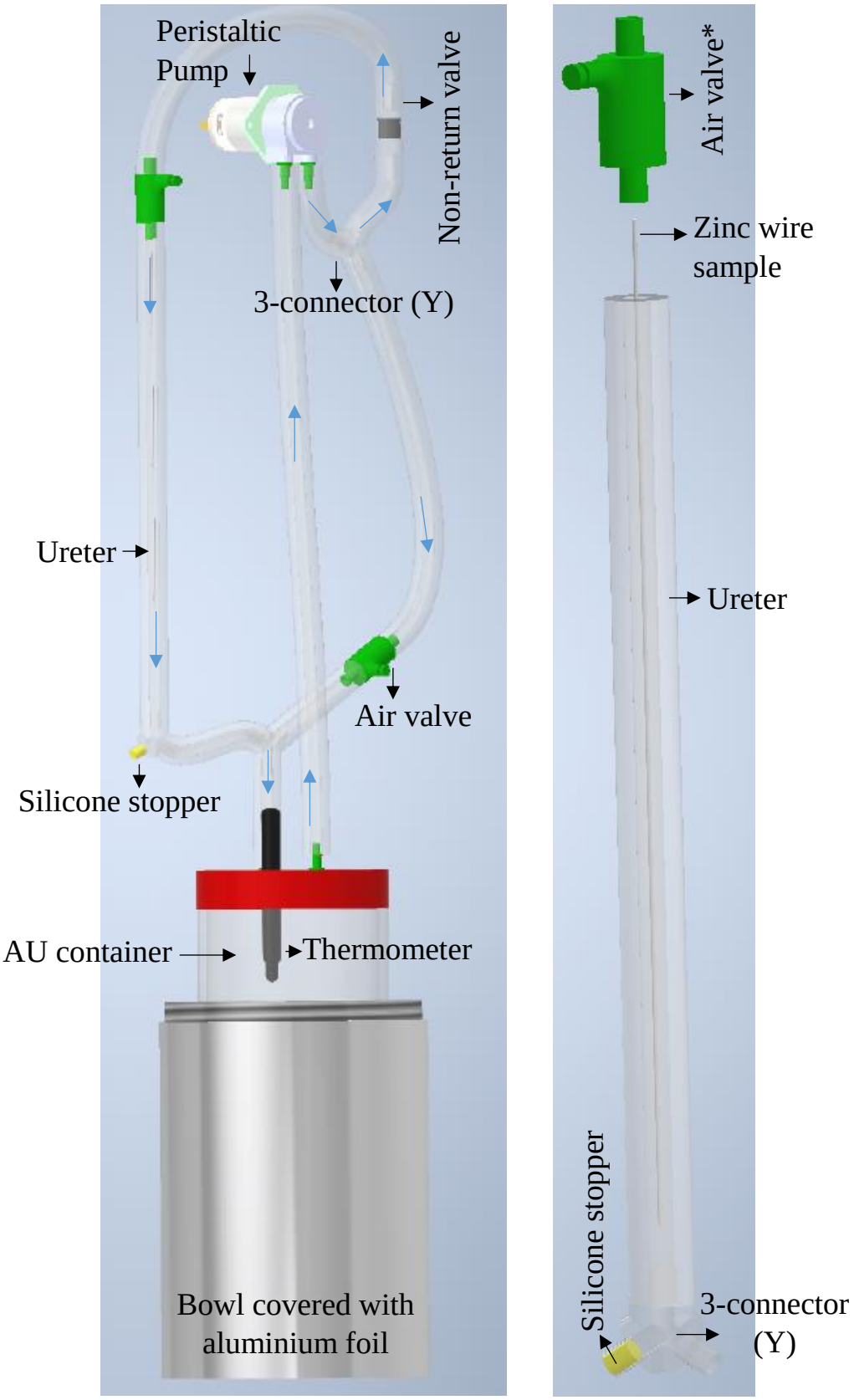

Figure 11. Final schematic diagram of (a) the set-up to immersion test. Blue arrows show direction of the flow or the AU artificial urine. (b) position of Zn wire sample in the simulated ureter.

3.4.2.2 Immersion corrosion test

Immersion corrosion testing was performed in order to analyse the corrosion layer in zinc wire samples generated in artificial urine solution over a period of 1 day and 3 days. The initial length and diameter of wire samples were 23.08 ± 0.14 cm and 1.00 mm, respectively.

Each day, 150 mL of the AU solution was changed to use fresh solution as possible and the pH of AU solution was measured with Universal Indicator Paper pH 1-14 (Metria CSPH 002 001).

Each sample was washed with distilled water for 2 min prior and after to immersion test. The specimens were weighed after drying and testing.

Immersion corrosion test was carried on two duration, one day and three days, each with three samples.

The corrosion rate (CRI) was calculated according to ASTM G1: *Standard Practice for Preparing, Cleaning and Evaluating Corrosion test specimens* using Eq. (5).

$$CRI = 8.76 \cdot 10^4 \frac{\Delta W}{A * t * \rho} \qquad \text{Eq. (5)}$$

where CRI is the corrosion rate (mm year^{-1}), ΔW (g) is the weight change (ΔW = initial weight – final weight), A(cm^2) is the surface area of the specimen, t (h) is the immersion time and ρ (g cm^{-3}) is the density of the metal.

Two samples for each period were then transferred to the SEM and EDS in order to reveal the compounds of the corrosion layer remnant and identify the diameter of the sample through twelve points along the wire with distance between them of 2 cm.

Finally, a statistical analysis was carried on with the SPSS 22.0 software to determine the significance of means of two data sets with T-student (for normalized distribution data) and U-mann Withney (for not normalized distribution data). The normalization was determined with Kruskal Wallis analysis. A p value < 0.05 was selected for statistical difference.

Chapter 4

Results

This chapter features the characterisation of Zn samples prior electrochemical and immersion tests, the microhardness results, the data obtained with the open circuit potential, potentiodynamic test, as well as, immersion test. Finally, describes the AU solution used in this study.

4.1 Characterisation of Zn samples prior corrosion testing

X-Ray diffraction patterns for both as-received Zn sheet samples and Zn wire samples can been seen in Figure 12. The diffractograms revealed the prominent peaks of the hexagonal crystal system of the zinc: (0 0 2), (1 0 0), (1 0 1) and (2 0 1) [146].

The diffractograms showed that Zn sheet pattern has more intensity than Zn wire pattern. For this reason, peaks (0 0 4) and (1 0 4) are weak in the Zn wire diffractogram. In the X-ray diffractograms, the characteristic zinc peaks are present with no extra peaks, so, impurities do not exist.

EDS was carried out to validate the purity of the samples (**Table 6**), showing the amount of oxygen, carbon, and zinc as average and full range as error of n = 3. Moreover, Figure 13 shows a smooth and homogeneous surface of Zn wire. Ideal surface to immersion test without grinding and polishing procedures.

Table 6. Elemental composition of Zn samples as received.

Element	Zn sheet sample (wt. %)	Zn wire sample (wt. %)
C	4.28 ± 0.71	11.20 ± 2.54
O	1.64 ± 0.30	4.65 ± 0.95
Zn	94.08 ± 1.00	84.15 ± 3.05

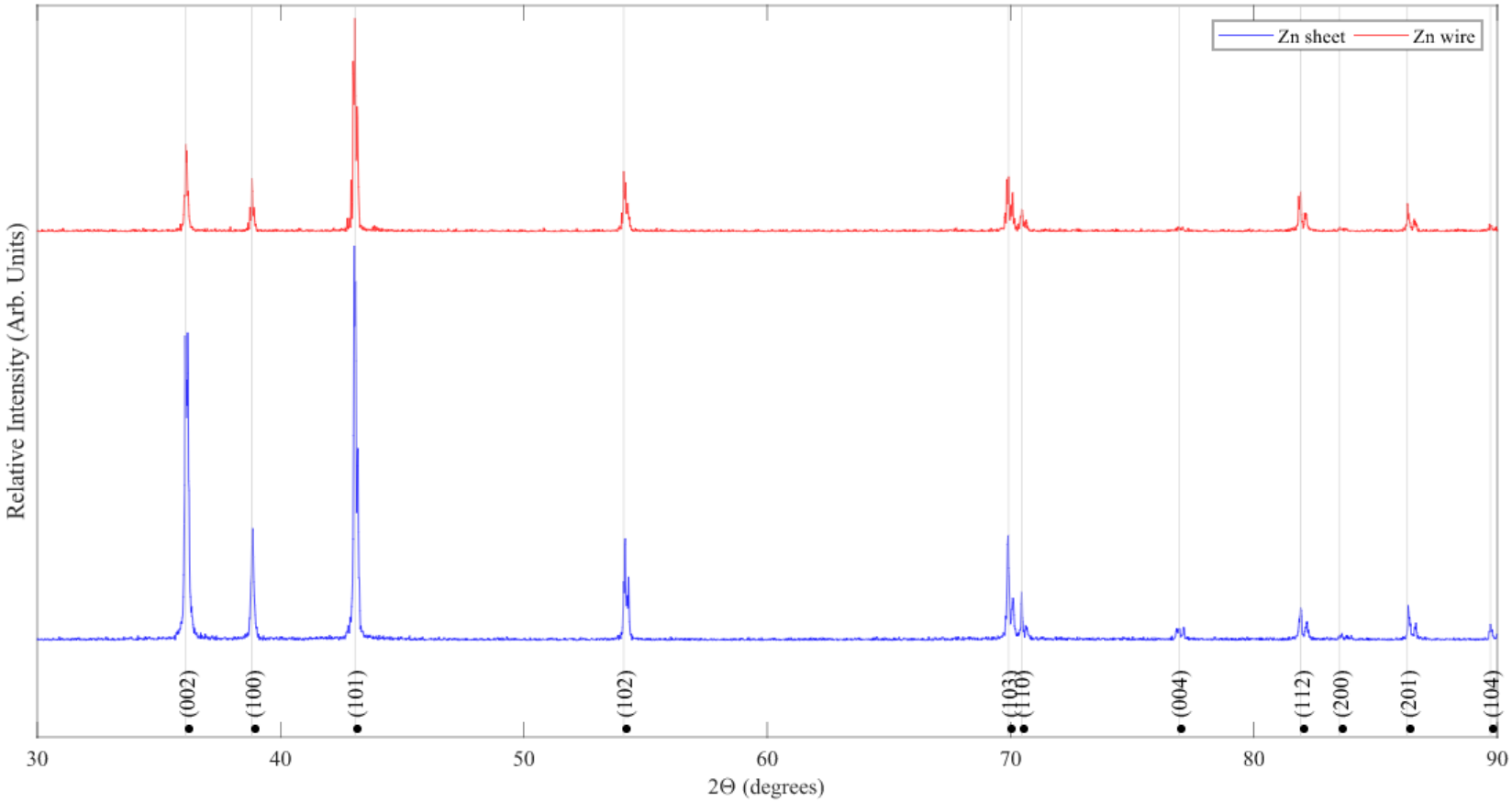

Figure 12. Diffractogram of as-received Zn sheet sample and Zn wire sample.

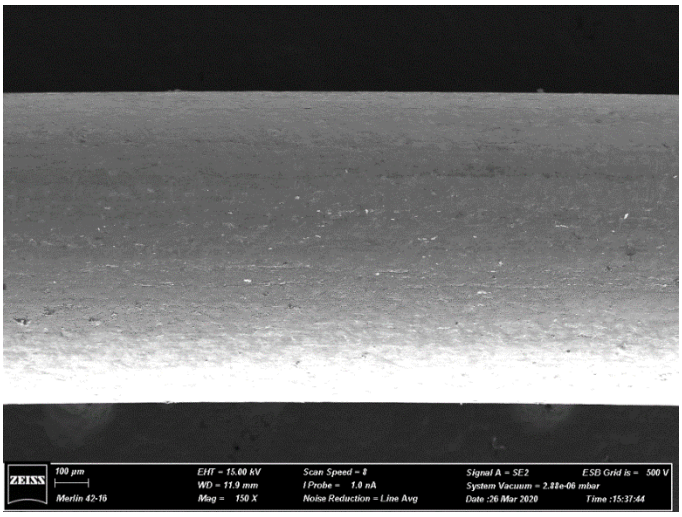

Figure 13. SEM image of the surface of Zn wire sample as received.

4.2 Microhardness test

Under the Vickers Scale and an applied load of 50 gf. The microhardness value obtained was 42.24 ± 2.72 HV, as result of n = 10, with average data and standard deviation.

The bar chart shown in Figure 14 compares the Vickers microhardness results from 4 studies; (ref. [93]), (ref. [105]), (ref. [108]) and the present study (TPS). The lowest HV is from the study 1 (ref. [93]), while TPS and study (ref. [108]) have the similar average data as the standard deviation.

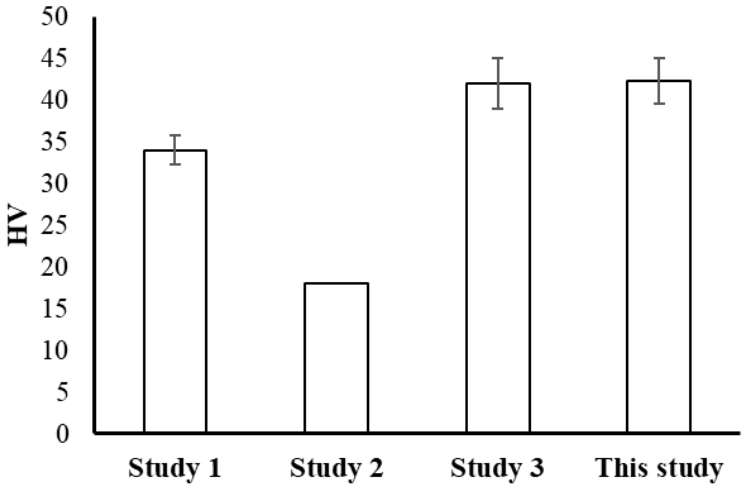

Figure 14. Comparison of Vickers microhardness results of study 1 (ref. [93]), study 2 (ref. [105]), study (ref. [108]) and this study.

4.3 Set-up used in the immersion test

The apparatus used in the immersion test followed the design criteria showed in the Table 5. However, during the test was observed the presence of bubbles in the artificial urine solution due to the use of air valves to control de flow rate of the solution through the simulate ureter.

4.4 AU solution

Under the same protocol presented in the methodology section, different artificial urine (AU) solutions can be obtained if the protocol is not followed correctly. The ideal AU solution is shown in Figure 15 (b), while variants of AU solutions are shown in Figure 15 (a, c-d).

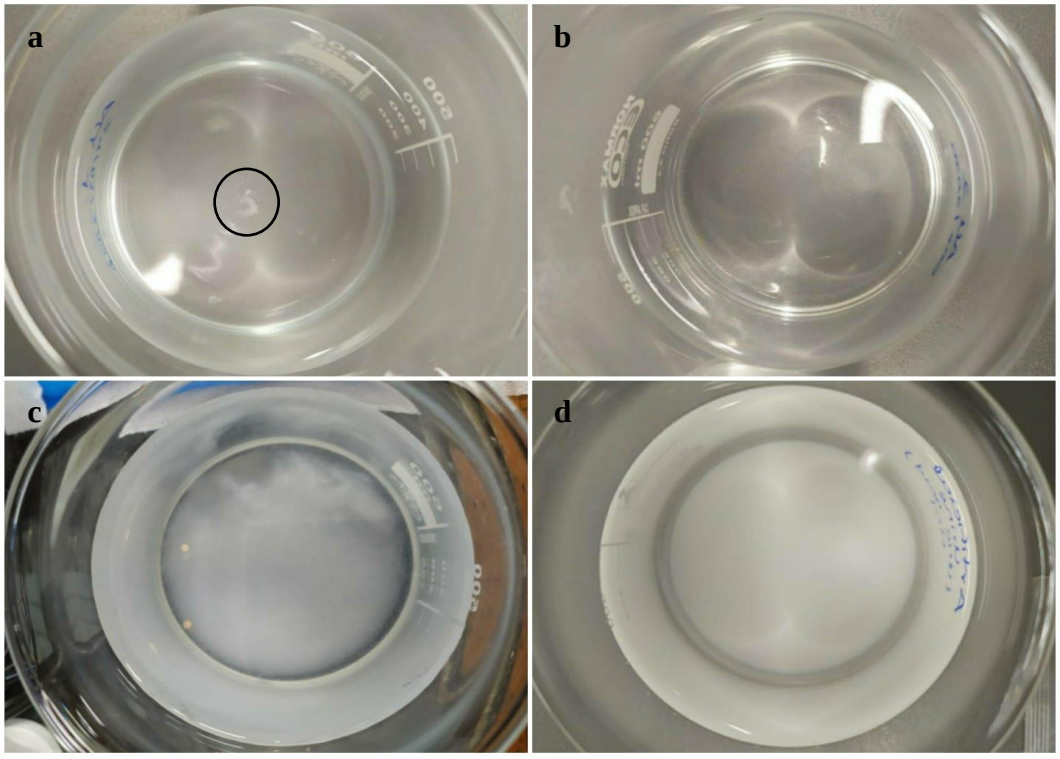

Figure 15. Result of the AU solution under the same protocol. (a) Powder chemicals were not crushed enough, (b) ideal AU solution, (c) Tris solution added on the chemical powder mixture and (d) the HCl used was contaminated.

Under the immersion test, the pH was taken to identify possible variations as function of the immersion time, 1 day and 3 days. Since a pH-meter cannot be used

due to technical issues, the Universal Indicator Paper pH 1-14 did not detect any evident change in the pH (Figure 16).

Possibly, the pH of the AU solution alkalinises in the day 1 and more after 3 days in the AU solution, because the indicators papers after both immersion time are more dark green than the prior papers, as can be observed in the Figure 16(b) and Figure 16 (c), respectively. However, it was not confirmed with another instrument.

This means that the pH of the AU solution prior and after immersion whatever time of immersion is nearly constant to 7, with a little increase to 8, however, any considerable change was not be able to identify.

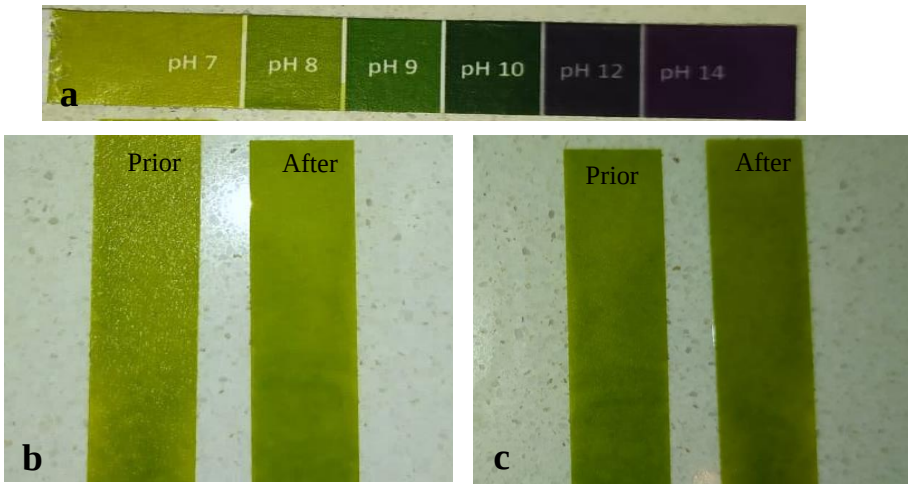

Figure 16. Results of pH of prior and after immersion test (a) Reference colour bar of the Universal Indicator Paper pH 1-14, (b) results over 1 day, (c) results over 3 days.

4.5 Electrochemical corrosion analysing test

The corrosion resistance of the Zn sheet samples was evaluated by electrochemical tests: open circuit potential (OCP) and potentiodynamic test (PDP). Under OCP (Figure 17), the voltage in all the Zn samples tended to a constant value after 2800 s. However, the voltage of the sample C increased at 1200 - 2000 s, due to presence of bubbles between reference electrode and exposed area of the specimens with the AU solution, as was observed only in this test. The voltage in sample C dipped and then acquired the voltage trend.

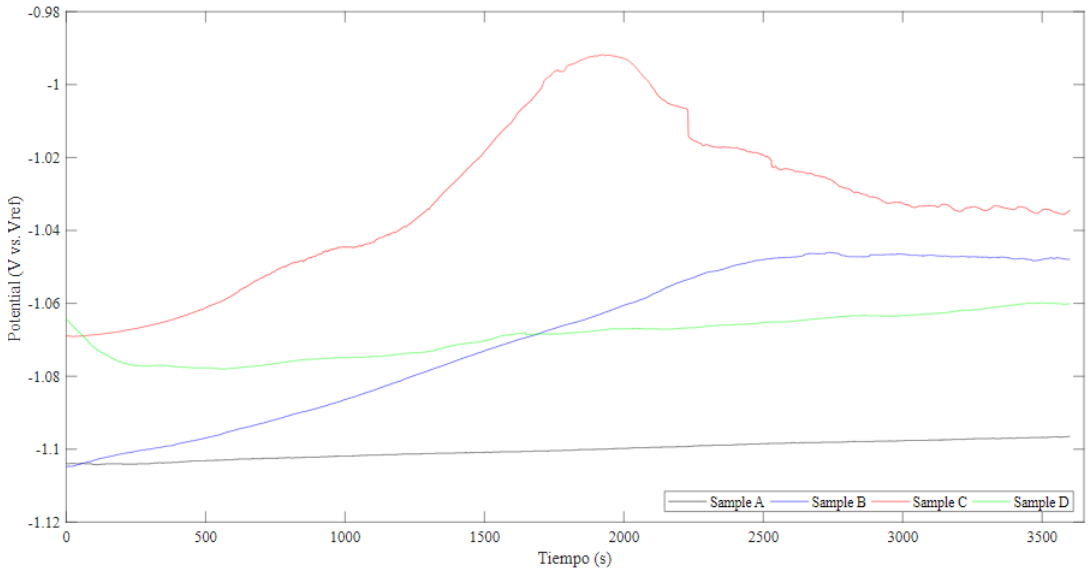

Figure 17. OCP plots of the n = 4 Zn sheet samples, in artificial urine solution. Potential vs. time.

Figure 18 shows the PDP curves for the Zn sheet samples, when exposed to AU solution. In the passive region, the current continues to rise till a potential of ~ V_{OCP} + 300 mV, when the current decrease till a potential of -1.05 V. At this point, the current increases drastically, changing the gradient of the slope, and the material enters in the transpassive dissolution.

Additionally, Figure 18 shows a typical curve of passivation behaviour in the Zn samples. The passivity is attributed to the presence of a passive film, the formation of the ZnO layer [14]. The presence of the biofilm inabilities the dissolved oxygen to reach the surface, leading to a reduction in metal ion dissolution [17]. After a Tafel extrapolation, the CRE obtained in this work was 0.10 ± 0.04 mm/year. Table 7 summarizes the corrosion parameters derived from PDP: E_{corr}, i_{corr} and corrosion rate.

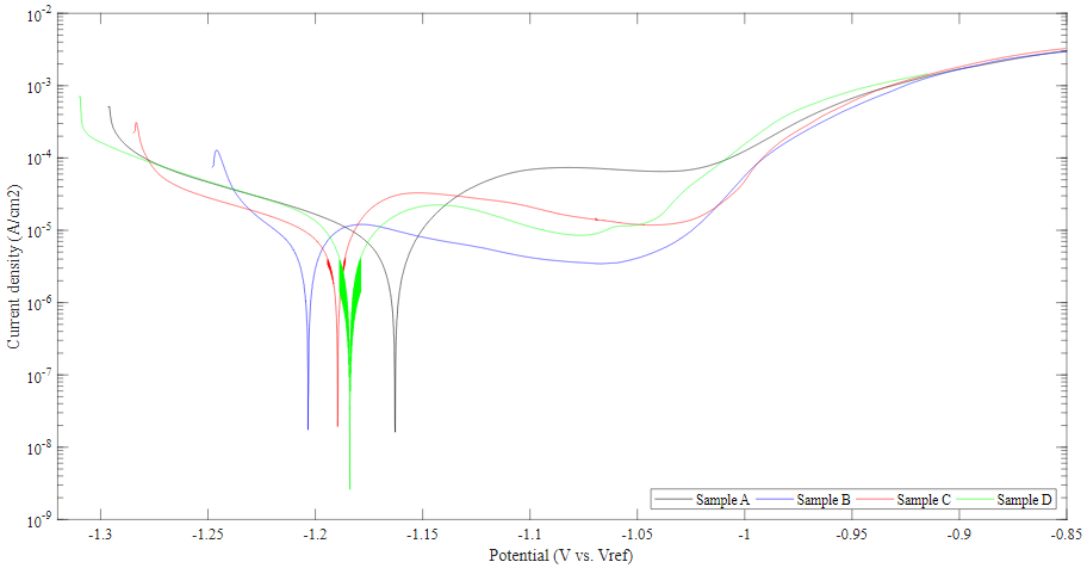

Figure 18. Potentiodynamic plots of n = 4 Zn sheet samples in artificial urine solution. Current density vs. potential.

Table 7. Corrosion parameters calculated from the potentiodynamic curves.

Sample	OCP (V vs. SCE)	E_{corr} (V)	I_{corr} (µA/cm^2)	Corrosion rate (mm/year)
A	-1.10	-1.16	6.21	0.09
B	-1.05	-1.20	3.96	0.06
C	-1.04	-1.19	7.07	0.11
D	-1.06	-1.18	9.36	0.14

After the polarisation test, the surface characterisation was carried on. When the potentiodynamic scan was stopped, it was noticed that the AU solution produced three circumferences identifiable in the sample surface as shown in the SEM images in Figure 19 (a-c).

Diameter of each circumference is: $\emptyset = 4.82 \pm 0.36\ mm$, $\emptyset = 7.37 \pm 0.16\ mm$ and $\emptyset = 8.04 \pm 0.13\ mm$, inner, intermediate and external diameter, respectively. In each circumference was identifying the elemental composition of the corrosion layer on the Zn samples, in specific zones (Figure 19 (d)), to compare differences between them.

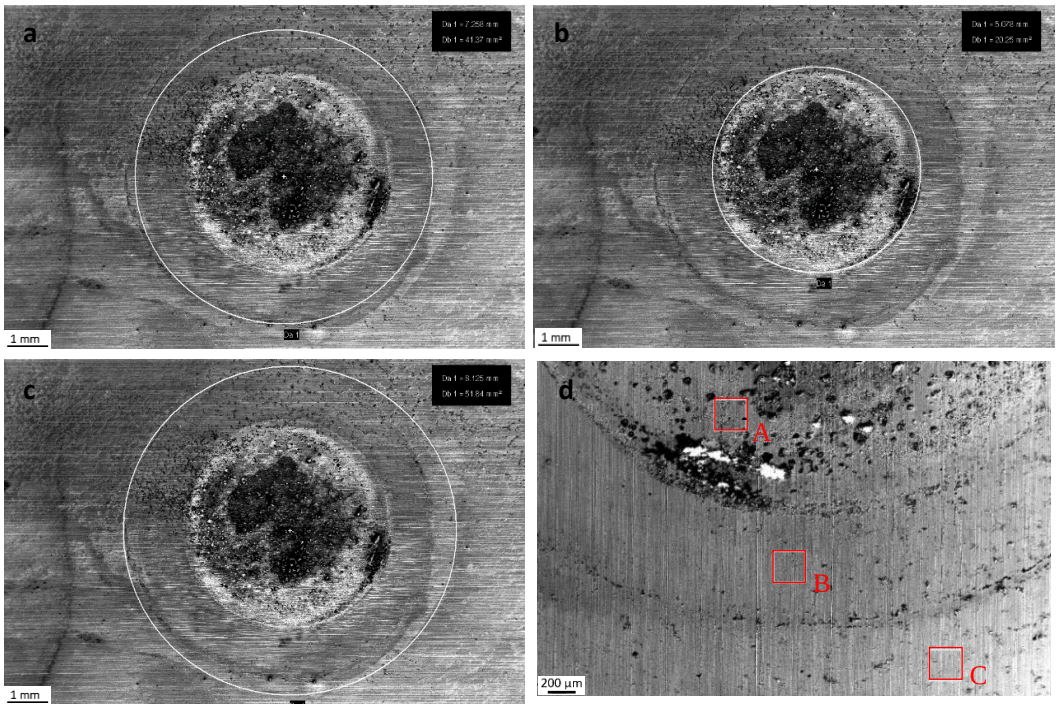

Figure 19. SEM images showing the typical diameter of the circumferences produced by the AU solution on Zn sheet samples after polarisation. (a) Inner circumference, Zone A. (b) Intermediate circumference, Zone B. (c) External circumference, Zone C. (d) Location of each EDS area on each zone.

Table 8 summarizes the elemental composition (wt. %) of corrosion products of Zn zones from EDS (Figure 19 (d)). Figure 20 shows the comparison of the elemental composition (wt. %) of Zn sheet samples as received, and the three zones identified after the PDP test. Only the C, O and Zn elements was taken account. No difference was observed in the elemental composition of C, O and Zn, between the initial surface prior tests and the zones: inner, intermediate and external, after tests.

Table 8. Elemental composition (wt. %) of corrosion products, n =4 of Zn sheet samples after polarisation test. Typical zones showed in Figure 19(d); average and standard deviation.

Zone	C	O	Si	P	S	K	Ca	Zn
A	4.48 ± 0.86	2.82 ± 1.37	0.32 ± 0.14	0.64 ± 0.21	0.19 ± 0.27	0.30 ± 0.42	0.10 ± 0.13	91.18 ± 3.12
B	3.71 ± 0.96	2.95 ± 0.96	0.23 ± 0.11	0.75 ± 0.16	0.12 ± 0.16	0.16 ± 0.22	0.17 ± 0.23	91.93 ± 2.62
C	4.92 ± 1.48	2.92 ± 1.97	0.23 ± 0.11	0.72 ±0.49	0.06 ± 0.08	0.17 ± 0.24	0.12 ± 0.17	90.88 ± 4.33

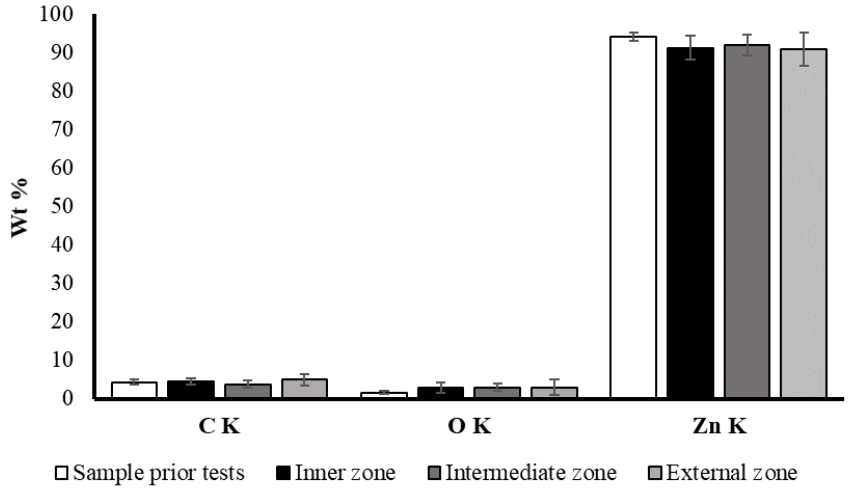

Figure 20. Elemental composition (wt. %) comparison between samples prior test, and zones identified after PDP tests in AU solution regarding to C, O and Zn elements. Average value and standard deviation as error.

Focusing in the inner circumference, both SEM images and EDS were done to identify possible crystallizations and anchor zones to encrustation. Table 9 describes the elemental composition of the specific zones showed in Figure 21.

Table 9. Elemental composition (wt. %) of corrosion products of Zn after polarisation test. Zones showed in Figure 21.

Zone	C	N	O	Si	P	S	Cl	K	Ca	Zn
A	04.46	-	04.02	00.15	00.92	00.06	00.15	00.25	00.21	89.79
B	05.98	01.37	20.71	00.12	06.04	00.52	00.54	00.47	00.07	64.18
C	05.09	-	25.07	00.15	08.89	-	-	-	-	60.81
D	03.45	-	02.22	00.29	00.60	-	-	-	-	93.45
E	09.39	03.18	31.30	00.12	10.59	-	01.81	01.68	01.13	40.80
F	10.08	02.92	16.04	00.12	02.14	0.13	00.35	00.64	00.23	67.34
G	08.36	02.30	16.85	00.35	08.77	00.07	01.22	01.69	01.31	59.08
H	09.57	02.27	21.98	00.83	03.68	-	00.06	02.32	00.28	59.01
I	03.37	-	01.67	00.10	00.56	-	-	-	-	94.29
J	07.22	-	30.96	00.10	09.75	-	-	-	-	51.97

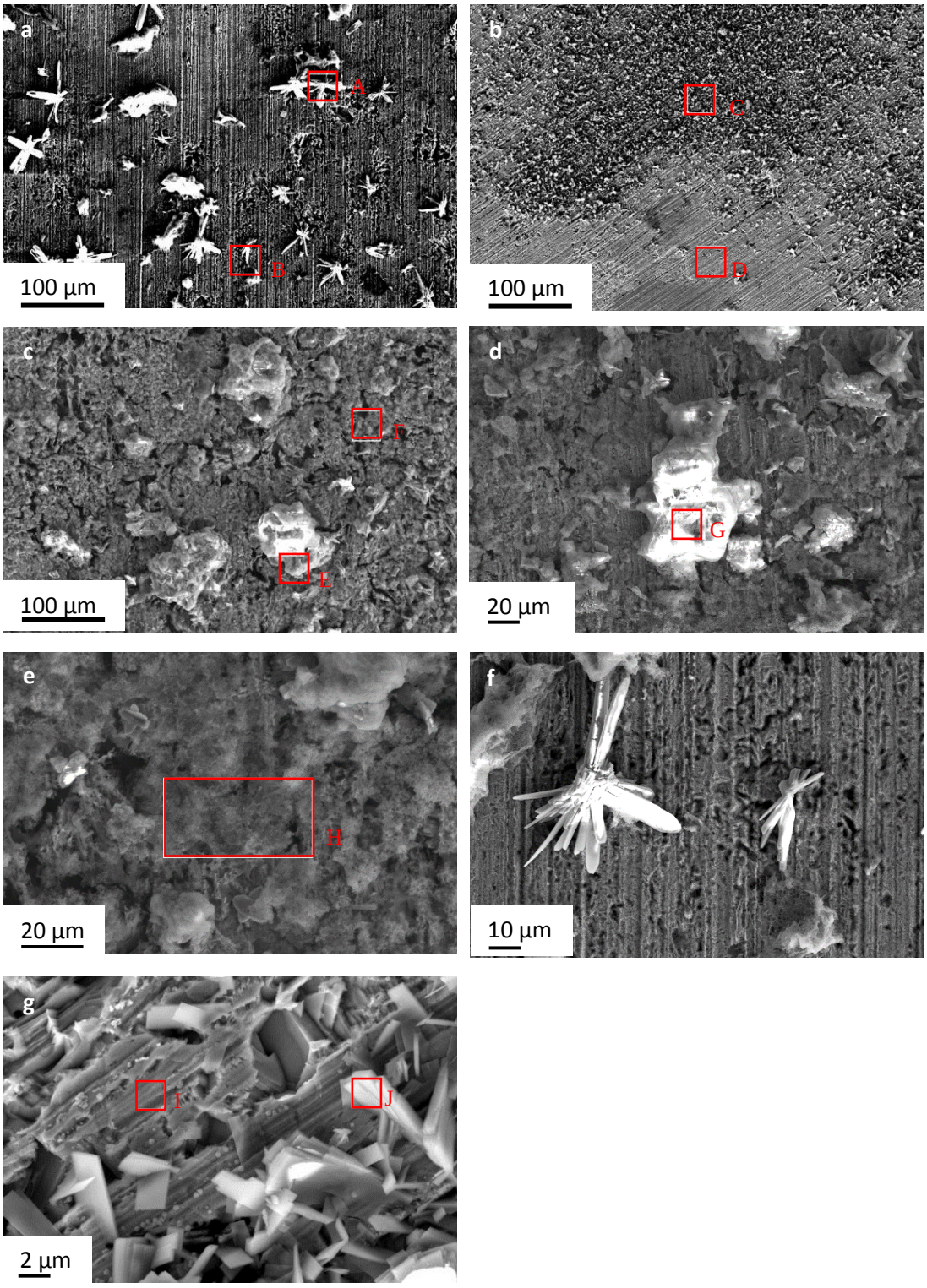

Figure 21. SEM micrographs showing the surface morphologies of Zn sheet samples after potentiodynamic testing in artificial urine solution and subsequent rinsing and sonication in ethanol at (a-c)500 X. (d) 1K X. (e, f) 2K X and (g) 10K X.

4.6 Immersion corrosion analysing test

The corrosion resistance of the Zn wire samples was evaluated by immersion corrosion test in a simulated ureter tract a period of 1 day and 3 days. The corrosion rate was calculated using the Eq. (5) and was registered in Table 10. Figure 22 compares the corrosion rates acquired in the electrochemical and immersion tests, showing the average data and the range as the error. The corrosion rate obtained in the immersion test for 3 days reveals a mass increase, while the other corrosion rates are related with mass loss.

Variation in the diameter along the zinc wire is presented in the Figure 23. Samples in both immersion times present decreases in their diameter on the twelve points registered. The decrease of the diameter of samples in 3 days remains nearly constant along the wire. In contrast, the decrease of the diameter of samples in 1 day varies along the wire. The diameter of the proximal end (location in the wire 1) was less than the diameter of the distal end (location in the wire 12) in the samples of 1 day in immersion test.

Table 10. Corrosion rate of n=3 samples of wire for each immersion time (1 day and 3 days); average data and range as error.

Average Corrosion rate (mm/year)			
1st day		3rd day	
0.08	+0.45 -0.24	-0.20	+0.41 -0.01

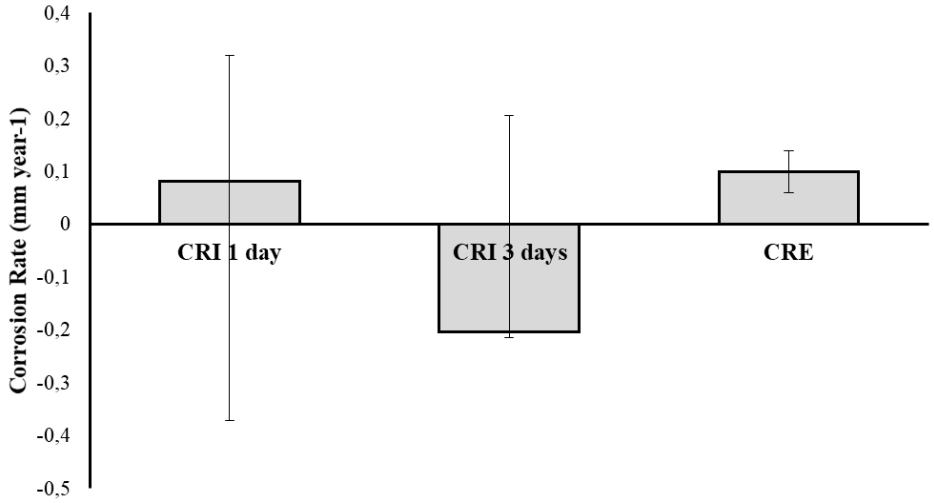

Figure 22. Comparison of corrosion rate obtained in electrochemical tests (CRE) and immersion time (CRI) in 1st day and 3rd days.

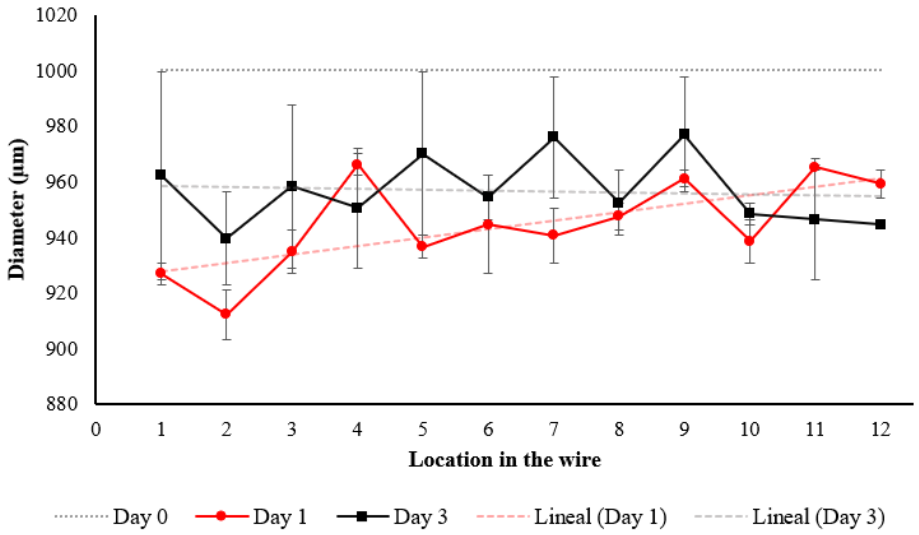

Figure 23. Average diameter for the zinc wire after 1 and 3 days of immersion test in AU solution, with range as error.

Another feature analysed was the thickness of the corrosion layer on the surface. Figure 24 displays the typical thickness of the corrosion layer from samples for both immersion times (1 day and 3 days). The corrosion layer decreases along the wire, thinner in the distal part (location in the wire 12) for both immersion time. Also, the corrosion layer retained on the surface becomes thicker when the immersion time increases.

The typical morphologies of the corrosion products on the surface along the wire samples in one day and three days of immersion time are shown in Figure 25 (a-d) and Figure 26 (a-d), respectively. Also, the boundaries of the wire samples were characterised with SEM and EDS as shown in the Figure 25 (e-h) and Figure 26 (e-h), respectively.

Difference in morphology was found between the samples after immersion testing in AU solution. This result can be considered as "no-uniform" corrosion occurring on each of the surfaces, due to the presence of porous and occasionally denser groups in the samples of immersion time of 3 days.

Then, elemental composition for each zone (zones A, B and C showed in Figure 25 and Figure 26) per each sample was analysed. Zone A was focused in the white areas, whereas zone B included areas with less corrosion product. Zone C represented the boundaries of the wire.

Differences were observed between the elemental composition recorded when samples were immersed to AU solution (Table 11). This was validated using T-student and U-mann Whitney analysis in function of time in the immersion sample (Table 12), in which the p-values of the Si in zone A, and the p-values of the elements C, O, Al and Zn were fallen below the threshold value of 0.05. However, in zone C was not obtained any difference in the elemental composition.

Moreover, Zone A and Zone C were compared in order to identify if elemental composition is significantly different according to the position of analysis in the sample (center part (Zone A) versus boundary (zone C)) as function of the immersion time (Table 13). In the samples of 1 day in AU solution only N, Mg, P, Ca, not showed differences; about the samples of 3 days in the AU solution, only Al did not show difference. The impact of this data is discussed in the next section.

Note that the presence of the Al and Si are not expected elements because neither are components of the as received samples nor to the AU solution used.

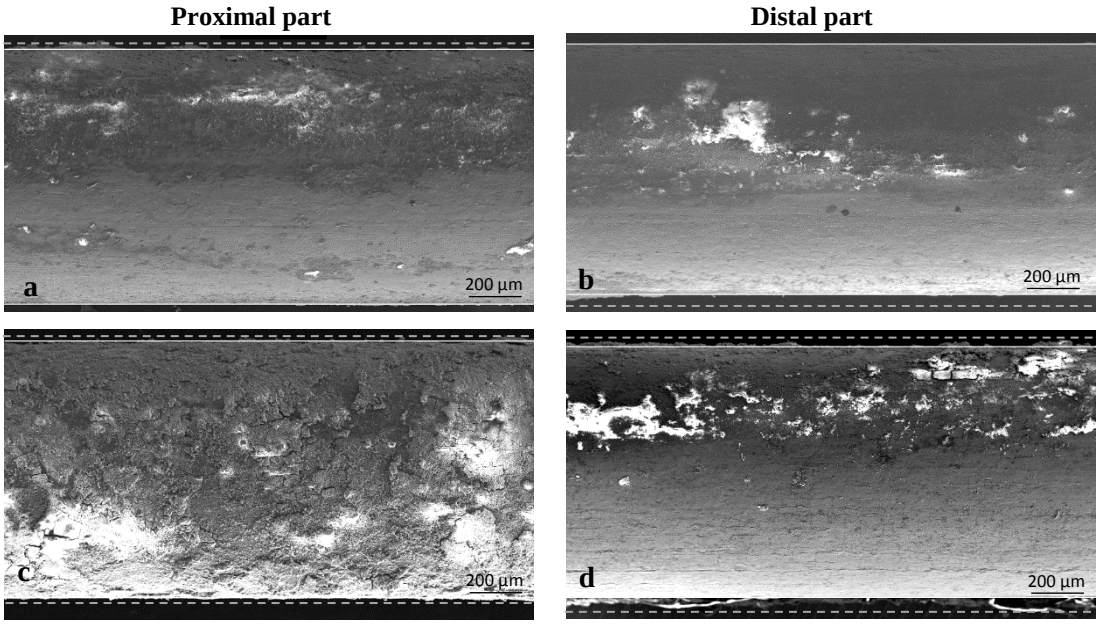

Figure 24. SEM images of corrosion layer develop on the surface of Zn wire samples after immersion test in AU solution, (a, b) 1 day and (c, d) 3 days in two points on the wire: proximal part (part near to the kidney, location in the wire 1) and distal part (part near to the bladder, location in the wire 12). Dotted lines mark the corrosion layer.

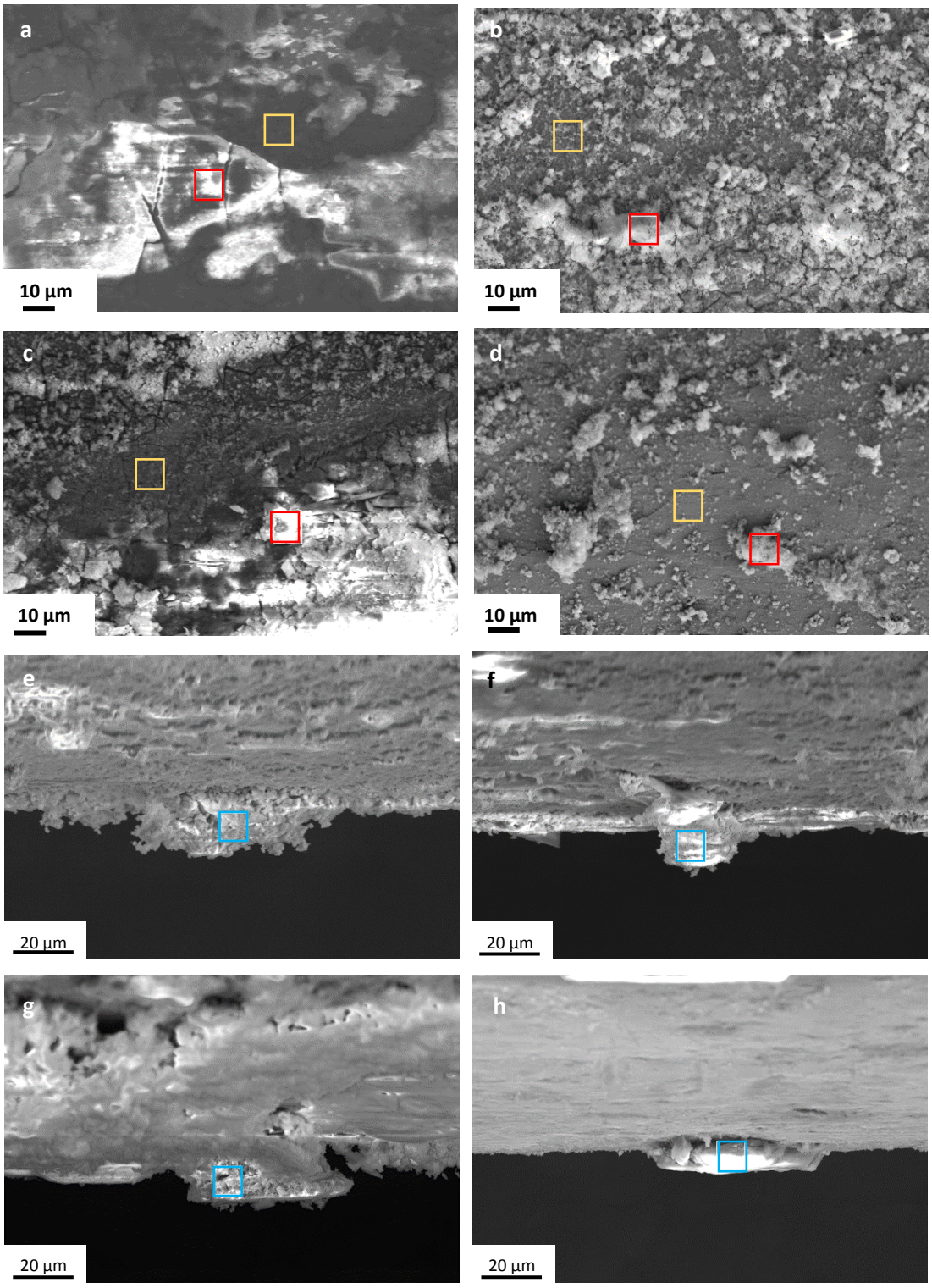

Figure 25. SEM images showing the typical morphology of (a-d) corrosion layer and (e-h) corrosion products in the boundaries of wire generated in samples in 1 day on immersion test in artificial urine solution. SEM images at 2 KX. Red squares (zone A), yellow squares (zone B) and blue squares (zone C).

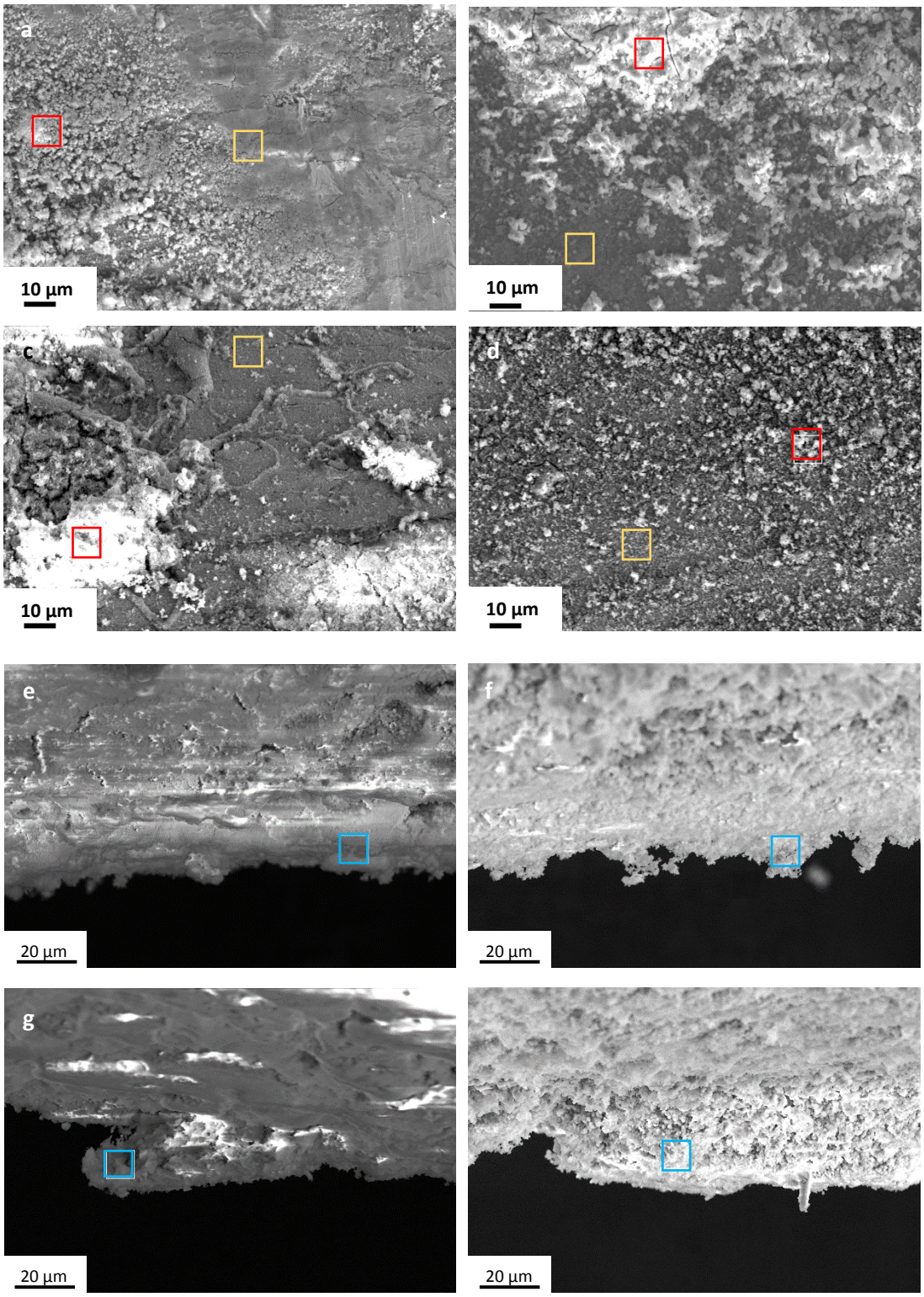

Figure 26. SEM images showing the typical morphology of (a-d) corrosion layer and (e-h) corrosion products in the boundaries of wire generated in samples in 3 days on immersion test in artificial urine solution. SEM images at 2 KX. Red squares (zone A), yellow squares (zone B) and blue squares (zone C).

Table 11. Composition obtained in EDS areas along the wire in the immersion test (1 day and 3 days samples) as a function of zones A, B and C shown in the Figure 25 and Figure 26. Data expressed as: average value and standard deviation of n = 24.

Zone	Immersion time	C	N	O	Mg	Al	Si	P	S	Cl	K	Ca	Zn
A	1 day	9.81 ± 0.85	1.65 ± 0.17	20.08 ± 1.61	0.27 ± 0.05	0.09 ± 0.01	0.15 ± 0.01	4.14 ± 0.77	0.57 ± 0.14	0.28 ± 0.05	0.45 ± 0.06	1.55 ± 0.29	61.01 ± 2.46
	3 days	11.71 ± 1.38	1.47 ± 0.14	17.39 ± 1.49	0.33 ± 0.03	0.40 ± 0.25	0.24 ± 0.04	3.36 ± 0.27	0.53 ± 0.15	0.24 ± 0.03	0.43 ± 0.03	1.49 ± 0.12	62.44 ± 2.68
B	1 day	8.34 ± 3.29	8.34 ± 3.80	8.35 ± 3.99	8.32 ± 4.43	8.34 ± 3.79	8.35 ± 5.39	8.35 ± 4.25	8.36 ± 3.58	8.35 ± 4.50	8.32 ± 3.55	8.33 ± 4.37	8.34 ± 3.44
	3 days	17.40 ± 2.62	3.31 ± 0.73	27.07 ± 1.03	0.46 ± 0.04	0.12 ± 0.03	0.29 ± 0.02	7.23 ± 0.71	1.35 ± 0.26	0.95 ± 0.27	0.85 ± 0.10	3.43 ± 0.36	37.55 ± 2.97
C	1 day	45.53 ± 2.72	2.46 ± 0.80	18.89 ± 1.09	0.78 ± 0.61	0.81 ± 0.39	0.23 ± 0.05	2.85 ± 0.50	0.56 ± 0.14	0.43 ± 0.10	0.59 ± 0.15	1.23 ± 0.10	25.33 ± 2.85
	3 days	44.76 ± 2.12	2.03 ± 0.34	17.78 ± 1.12	0.21 ± 0.04	2.40 ± 1.28	0.22 ± 0.07	3.15 ± 0.31	0.40 ± 0.06	0.28 ± 0.07	0.40 ± 0.03	1.59 ± 0.17	26.82 ± 2.62

Table 12. p-values from T-student* or U-mann Withney testing of comparison of the composition obtained in each zone along the wire as function of the immersion time. p-values>0.05 implies that no difference can be observed between the two datasets being compared.

Zone	C	N	O	Mg	Al	Si	P	S	Cl	K	Ca	Zn
A	0.248	0.453	0.232*	0.184	0.202	0.005	0.351*	0.954	0.707	0.760*	0.299	0.697*
B	0.015	0.644	0.004	0.603	0.002	0.298	0.065	0.488	0.299	0.204	0.248	0.000
C	0.826*	0.862	0.484*	0.885	0.794	0.603	0.618*	0.862	0.202	0.488	0.090	0.908

Table 13. p-values from T-student* or U-mann Withney testing of comparison between composition of zone A and zone C obtained in EDS along the wire in the immersion test where p-values>0.05 implies that no difference can be observed between the two datasets being compared.

Time of immersion test	C	N	O	Mg	Al	Si	P	S	Cl	K	Ca	Zn
1 day	0.000	0.817	0.013	0.065	0.033	0.037	0.525	0.021	0.028	0.033	0.954	0.008
3 days	0.000	0.010	0.000*	0.000	0.755	0.008	0.000*	0.000	0.045	0.000*	0.000*	0.004

Chapter 5

Discussion

5.1 Zn samples Degradation Resistance

The corrosion rates acquired in the electrochemical and immersion tests were lower than the corrosion rate of Zn samples in AU solution registered by Champagne *et al.* [136]. This difference is probably due to the use of different AU solution formulation.

Additionally, Figure 18 shows a typical curve of passivation behaviour in the Zn samples. The passivity is attributed to the presence of a passive film, the formation of the ZnO layer [108], in the electrochemical tests did in this work. The presence of the biofilm inabilities the dissolved oxygen to reach the surface, leading to a reduction in metal ion dissolution [147].

Furthermore, in this study, the negative corrosion rate of the immersion test under a period of 3 days implies an error in the experimental procedure used. The standard practice for cleaning the specimens to obtain the weight loss was not carried out correctly due to the samples stored for a long time due to technical issues, and the samples also were not re-weighted *n* times until the weight recorded at time *n-1* was equal to the weight at time *n*.

Another feature that can describe the degradation resistance of the Zn wire samples is the variation of the diameter along the wire (Figure 23). Since samples in both immersion times present decreases in their diameter, it shows a mass loss of the specimens; however, due to the incorrect determination of the weight loss, the mass loss cannot be corroborated. Also, the nearly constant decrease in the diameter of samples in 3 days, but major than 1 day, shows the growth of the corrosion layer, affirming the formation of layers to avoid corrosion.

However, the AU solutions used in the present study is different of the solution used by Champagne *et al.* [136]. The Zn samples were exposed to extremely complex corrosive medium. AU solution can alter the degradation behaviour and corrosion rates of the samples [108]. Therefore, the difference in the corrosion rates acquired and provided in the literature may also be related to the difference in solutions.

To improve the degradation rate of pure zinc in biomedical applications, several methods include coatings, surface film manipulation, alloying, and microstructure modification [148]. Also, further studies with long immersion tests might be done to analyse the corrosion behaviour of the Zn-based and Zn alloys samples.

5.2 Elemental composition of the corrosion layer of Zn samples

The pure Zn samples in artificial urine solution can have the formation of zinc oxide, zinc hydroxide, zinc carbonate, zinc phosphate and, calcium phosphate on the top layer as mentioned in the previous non-urinary studies [93, 108, 135] and, urinary study [136]. EDS analysis confirmed that the elemental composition of as received Zn samples (wire and sheet) included only Zn, C and, O (Table 6).

After the potentiodynamic test, the elemental composition did not show differences regarding the elements of as received Zn samples (Figure 18). Also, the formation of zinc oxide was corroborated (Figure 21 (f)) [136]. ZnO is an expected corrosion product due to the relation between the pH of the AU solution (pH 7) and the zinc Pourbaix diagram (Figure 6).

A high concentration of carbon on the boundaries of the wire (high concentration of C, zone C in Table 11) may be related to C-C, C-O(H) or, carbonate [108]. If the latter is present in the samples, the AU solution it is not acidic because carbonate dilutes in diluted acids. The presence of Zinc phosphate may affect the corrosion rates due to is used as a resistant coating in metal surfaces [149].

In the corrosion layer of the samples, the presence of Ca may produce calcification, thus, encrustation [136], and prompting the formation of urinary stones. Uric acid, calcium phosphate, struvite and calcium oxalate are the mainly compound of these stones [150].

However, the XPS analysis might confirm the formation of the zinc corrosion compounds mentioned previously.

In the immersion test, the significative difference (Kruskale Wallis or T-student, $p < 0.05$) was observed in the zone A (EDS area on white zones) about Si and the zone B (EDS area on dark zones) with O, Al and, P. In contrast, in the zone C, boundary along the wire samples, do not have a difference in the chemical composition.

Si and Al should not be presented in the elemental composition due to the Zn samples did not have impurities and the AU solution formulation did not include these elements. Probably, the samples after corrosion tests would be contaminated in contact with any surface metallic; but another reason that they are presented is not identified.

About the zone B, the difference of O along the samples implies that the oxidation does not happen homogeneous throughout the wire under the immersion tests.

On the other hand, according to the comparison between zone A and zone C, the elemental composition has a significant difference. In the immersion tests of 1 day, C, O, Al, Si, S, Cl, K, and Zn vary between the central area to boundaries; while under immersion test of 3 days, only Al does not have a statistical difference. These results mean that the reaction of the zinc samples with the AU solution would be affected by the immersion time.

After immersion test, the remnant thickness of the corrosion layer on the surface of specimens (Figure 24) increased for both immersion times. This result means that the reaction of the zinc samples with the AU solution would be affected by the immersion time. The corrosion layer was determined to be composed mainly of carbon (zone C in the Table 11) as determined by EDS.

The results make this project an approach to the elemental composition of the Zn-based samples under artificial solution with urological propose.

5.3 Mechanical properties of the Zn samples

The difference between the microhardness values (Figure 14) is a consequence of the purity of the Zn samples and the procedure to obtain the Zn specimens. Zang et al. [108] were the unique authors that used a commercially Zn wire with a purity of 99.99+ wt%, and for this reason, difference significative do not exist between the results obtained.

The literature showed that the microhardness and other mechanical properties as Yield strength, tensile strength, and ductility elongation of pure Zn could be improved significantly in Zn alloys with Mg, Al [93], Mn [105] and Li [108].

Nevertheless, while inserting and removing the ureteral stents is not recommend use force to prevent the creation of anchor zones for urinary tract infection, encrustation, and fractures along the stent [151]. So, some side-effects of ureteral stents can be avoided improving the mechanical properties of the material used.

5.4 AU solution

The purpose of controlling the pH was to regulate the acidity or alkalinity of the AU solution to use the information related to the Pourbaix diagram, redox states of the zinc as a function of pH. However, for technical issues, the use of a pH meter was not possible, so the Universal Indicator Paper pH 1-14 (Metria CSPH 002 001) was used.

The indicator paper used is not a reliable meter, it could not be stated whether alkalinisation was present in the AU solution. The chromatic perception is subjective and can be wrongly perceived. Furthermore, the sensitivity of the tool does not allow identifying slight variations during all the time of the experiments.

Zhang, X. [134] affirms that zinc degradation does not produce hydrogen bubbles or increase alkalinity. Also, the presence of the tris solution in the formulation of AU solution used will not allow the shift in the pH. Since Figure 16 suggests alkalinisation in the AU solution during the immersion test, the result can be associated with the use of a not reliable meter and not for the increase of hydrogen ions in the AU solution.

5.5 Set-up used in the immersion test

Since the set-up design followed correctly the design criteria, the apparatus was a helpful tool to simulate the upper urinary tract and to do the immersion tests.

However, the following recommendations can be drawn to further studies;

(i) Do not use air valves to control the flow rate of the solution through the system. At times, air valves generate air bubbles. The presence of air bubbles

causes turbulent flow and increases the O in the urinary tract, affecting the control corrosion of the metallic samples

(ii) Include electrodes to control more variables like current, voltage, and pH.

(iii) If the simulated ureter is made of silicone pipe, it should be changed for each immersion test. This action prevents contamination of the new sample due to the remaining corrosion product adhering to the ureter of the previous sample that was removed.

Chapter 6

Conclusion

In this study, pure Zn samples have been investigated as possible candidates for biodegradable stent applications. Analysing the results obtained, the following conclusions can be drawn;

(i) The purity of the zinc samples corroborated with XRD demonstrates that the samples used can be the source of Zn matrix to mechanical alloy with other elements to improve the mechanical properties of the material. The micro-hardness value was 42.24 ± 2.72 HV in the pure Zn.

(ii) Corrosion rates were measured by potentiodynamic polarisation and immersion tests using artificial urine solution. The corrosion rates of Zn in electrochemical test was 0.10 ± 0.04 mm/year, and in immersion test under period of 1 day and 3 days were 0.08 (+0.45 and -0.24) mm/year and -0.20 (+0.41 and -0.01) mm/year, respectively. However, the corrosion rates implied a slower degradation ratio than results of other studies.

(iii) In this study, the negative corrosion rate of the immersion test under a period of 3 days implies an error in the experimental procedure used, because the degradation products that are still stuck to the Zn sample surface increase the mass. However, the variation of the diameter along the wire samples shows the degradation of the samples in the AU solution.

(iv) The nearly constant decrease in the diameter of samples in 3 days, but higher than day 1, implies the growth of a corrosion layer. Moreover, the diameter reduction for Zn samples displayed a relationship between the mass loss and immersion time.

(v) SEM images and elemental composition of the samples did not reveal a uniform corrosion, mainly due to the presence of a compacted passive layer on their surface.

(vi) ZnO layer affects the degradation rate of the samples. ZnO reduces the reaction between the ionic content of the urine solution and the surface of the metallic specimens.

(vii) The presence of Ca in the corrosion layer of the specimens is an undesirable result due to increases in the anchor zone to encrustation and production of urinary stones.

(viii) The EDS analysis confirmed the presence of the elements that generate corrosion products like calcium phosphate, zinc oxide, zinc chloride hydroxide, and zinc carbonate.

(ix) Si and Al, (0.15 – 8.35 and 0.09 – 8.34)[15], respectively, should not be presented in the elemental composition due to the Zn samples did not have impurities and the AU solution formulation did not include these elements.

(x) The AU solution used was a complex corrosive medium; however, variation in the pH was not identified due to the AU formulation control possible change in pH with the use of tris solution. Also, the zinc degradation does not produce hydrogen bubbles or increase alkalinity [134].

(xi) The apparatus designed to simulate the upper urinary tract and perform the immersion tests met all design and function criteria as expected.

Then, Zn is a new challenge to biodegradable applications in the urology field. However, the corrosion rate should be improved with surface film manipulation, alloying, and microstructure modification. Also, further studies with long immersion tests might be done to better control of the corrosion behaviour of the based-Zn samples.

[15] Range of average values registered in Table 11.

Future medium-term works

Zn is a new challenge to biodegradable application in the urology field. In order to optimise and improve the contributions of this project there are further studies that should be carried out.

- Study and characterise Zn-alloys, in order to investigate the degradation behaviour in the same AU solution.
- In vitro studies use the AU solution proposed by Sarigui *et al.* [13] to more approach to the human urine and improve the measurement of pH with the use of a precision instrument.
- Study and characterise the cytocompatibility in cellular cultures such as, in order to study in vitro degradation resistance and cell conditions.
- Further study on the biodegradation behaviour of the Zn samples using longer immersion tests.
- Modify the surface of the Zn-based samples to remove the ZnO formation to improve the corrosion rate.
- Elaborate a new set-up to mimic the ureteral system considering not use air valves, a changeable simulated ureter with funnel and, undulated shape made of silicone pipe, simulate different urological complications, and avoid reuse of AU solution used in the immersion time.
- XPS analysis, as another alternative to EDS, to identify correctly the compounds of corrosion products.
- Implement the characterisation of different urological complications that need a ureteral stent as the solution, for instance, obstructions throughout the ureter.
- Study the effect of the funnel and, undulated shape of the ureter may suggest new designs of ureteral stents.
- Avoid reuse of the urine solution to mimic the fresh production of urine by the bladders.

References

[1] A. Mosayyebi, C. Manes, D. Carugo y B. K. Somani, «Advances in Ureteral Stent Design and Materials,» *Current urology reports,* vol. 19, nº 5, 2018.

[2] A. M. Acosta-Mirand, J. Milner y T. Turk, «The FECal double-J: a simplified approach in the management of encrusted and retained ureteral stents,» *Journal of Endourology,* vol. 23, pp. 409-415, 2009.

[3] K. Nikkhou, H. Kaimakliotis y D. Singh, «Fractured Retained Ureteral Stent in a Patient Lost to Follow-Up,» *Journal of Endourology,* vol. 25, pp. 1829-1830, 2011.

[4] J. S. Lam y M. Gupta, «Tips and Tricks for the Management of Retained Ureteral Stents,» *Journal of Endourology,* vol. 16, pp. 733-741, 2002.

[5] A. Barros, C. Oliveira, E. Lima, A. Duarte, K. Healy y R. Reis, «Ureteral Stents Technology: Biodegrdable and Drug-Eluting Perspective,» de *Comprehensive Biomaterials II*, Elsevier, 2017, pp. 793-812.

[6] H. B. Joshi, A. Stainthorpe, R. P. MacDonagh, F. X. Keeley y A. G. Timoney, «Indwelling Ureteral Stents: Evaluation of Symptoms, Quality of Life and Utility.,» *Journal of Urology,* vol. 169, 2003.

[7] G. Katarivas Levy, J. Goldman y E. Aghion, «The prospects of Zinc as a structural material for Biodegradable Implants-A Review Paper,» *Metals,* vol. 7, 2017.

[8] J. E. Hall and A. C. Guyton, Guyton and Hall - Textbook of Medical Physiology, Jackson, Mississippi: Elsevier, 2016.

[9] L. H. &. e. Avendaño, Nefrología clínica, Editorial Médica Panamericana, 2003.

[10] G. J. Tortora y B. Derrickson, Principles of anatomy and physiology, United States of America: WILEY, 2017.

[11] K.-W. Kim, Y. H. Choi, S. B. Lee, Y. Baba, H.-H. Kim y S.-H. Suh, «Analysis of Urine Flow in Three Different Ureter Models,» *Computational and Mathematical Methods in Medicine,* 2017.

[12] G. R, «The Time-Distance Diagram of the Ureteral Transport,» de *Urodynamics*, Berlin, Heidelberg, Springer, 1985, pp. 102-119.

[13] N. Sarigul, F. Korkmaz y I. Kurultak, «A New Artificial Urine Protocol to Better Imitate Human Urine,» *Scientific reports,* vol. 9, nº 20159, 2019.

[14] J. Y. Lock, E. Wyatt, S. Upadhyayula, A. Whall, V. Nuñez, V. I. Vullev y H. LIu, «Degradation and antibacterial properties of magnesium alloys in artificial urine for

potential resorbable ureteral stent applications,» *J Biomed Mater Res,* vol. 102, nº 3, pp. 781-792, 2014.

[15] N. Morris, D. Stickler y R. McLean, «The development of bacterial biofilms on idwelling urethral catheters,» *World J Urol* , vol. 17, nº 6, pp. 345-350, 1999.

[16] S. King Strasinger y M. Schaub Di Lorenzo, Urinalysis and Body Fluids, Philadelphia: E.A. DAVIS COMPANY, 2008.

[17] L. Haddad, «Synthetic urine and method of making same». United States of America Patente 7109035 B2, 19 September 2006.

[18] N. Sarigul, F. Korkmaz y I. Kurultak, «A New Artificial Urine Protocol to Better Imitate Human Urine,» *Scientific Reports,* vol. 9, 2019.

[19] T. Brooks y C. W. Keevil, «A simple artificial urine for the growth of urinary pathogens.,» *Letters in applied microbiology,* vol. 24, pp. 203-206, 1997.

[20] S. Chutipongtanate y V. Thongboonkerd, «Systematic comparisons of artificial urine formulas for in vitro cellular study,» *Analytical Biochemistry,* Vols. %1 de %2110-112, p. 402, 2010.

[21] J. Hall y K. D. Linton, «Obstruction of the upper and lower urinary tract,» *Surgery- Renal and Urology,* vol. 26, nº 5, pp. 197-202, 2008.

[22] D. K. Newman, E. S. Rovner y A. J. Wein, Clinical Application of Urologic Catheters, Devices and Products, Philadelphia: Springer International Publishing, 2018.

[23] G. M. Preminger, «MSD Manual - Urinary Tract Obstruction,» October 2019. [En línea]. Available: https://www.msdmanuals.com/home/kidney-and-urinary-tract-disorders/obstruction-of-the-urinary-tract/urinary-tract-obstruction. [Último acceso: 18 December 2019].

[24] K. Reyner, A. C. Heffner and C. H. Kasrvetski, "Urinary obstruction is an important complicating factor in patients with septic shock due to urinary infection," *American Journal of Emergency Medicine,* 2016.

[25] L. E. Nicolle, «Urinary Tract Infection,» *Critical Care Clinics,* vol. 29, pp. 699-715, 2013.

[26] C. Türk , A. Petrík, K. Sarica, C. Seitz, A. Skolarikos, M. Straub y T. Knoll, «EAU Guidelines on Interventional Treatment for Urolithiasis,» *European Urology,* vol. 69, nº 3, pp. 475-482, 2016.

[27] G. Mohan Sali y H. B. Joshi, «Ureteric stents: Overview of current clinical applications and economic implications,» *International Journal of Urology,* 2019.

[28] A. B. Locke, «Urinary Tract Infection,» de *Integrative Medicine,* Elsevier, 2018, pp. 211-217.e2.

[29] D. Lange y B. H. Chew, «Update on ureteral stent technology,» *Therapeutic Advances in Urology,* vol. 1, nº 3, pp. 143-148, 2009.

[30] C. Patel, D. Loughran, R. Jones, R. Abdulmajed y I. Shergill, «The resonance® metallic ureteric stent in the treatment of chronic ureteric obstruction: a safety and efficacy analysis from a contemporary clinical series,» *BMC Urology*, vol. 17, pp. 16-20, 2017.

[31] A. Barros, C. Oliveira, A. Jacinta, R. Autorino, R. Reis, A. Duarte y E. L. Lima, «Homogeneous biodegradable ureteral stent: In vivo evaluation in a porcine model,» *European Urology Supplements*, vol. 16, nº 4, 2018.

[32] J. D. Denstedt, G. Reid y M. Sofer, «Advances in ureteral stent technology,» *World Journal of Urology*, pp. 237-242, 2000.

[33] D. Lange, S. Bidnur, N. Hoag y B. H. Chew, «Ureteral stent-associated complications - where we are and where we are going,» *Nature Reviews Urology*, vol. 12, nº 1, pp. 17-25, 2014.

[34] A. Hudecki, G. Kiryczynski y M. J. Los, «Chapter 7 - Biomaterials, Definition, Overview,» de *Stem cells and biomaterials for regenerative medicine*, Academic Press, 2019, pp. 85-89.

[35] H. K. Mardis, M. Kroeger, J. J. Morton y J. Donovan, «Comparative evaluation of materials used for internal ureteral stents,» *Journal of Endourology*, vol. 7, nº 2, pp. 105-115, 1993.

[36] A. Hudecki, G. Kiryczynski y M. J. Los, «Chapter 7 - Biomaterials, Definition, Overview,» de *Stem cells and biomaterials for regenerative medicine*, Academic Press, 2019, pp. 85-89.

[37] P. D. Zimskind, T. R. Fetter y J. L. Wilkerson, «Clinical use of long-term indwelling silicone rubber ureteral splints inserted cytoscopically,» *Journal of Urology*, vol. 97, nº 5, pp. 840-844, 1967.

[38] X. S. Chauhan, R. Bansal y M. Ahuja, «Comparison of Efficacy and Tolerance of Short-Duration Open-Ended Ureteral Catheter Drainage and Tamsulosin Administration to Indwelling Double J Stents Following Ureteroscopic Removal of Stones,» *Hong Kong Medical Journal*, vol. 21, nº 2, pp. 124-130, 2015.

[39] L. Huang, X. Wang, Y. Ma, J. Wang, X. Tao, L. Liao y J. Tan, «A Comparative Study of 3-week and 6-week Duration of double-J Stent Placement in Renal Transplant Recipients,» *Urologia internationalis*, vol. 89, nº 1, pp. 89-92, 2012.

[40] M. L. Stoller, B. F. Schwartz, J. R. Frigstad, L. Norris, J. B. Park y M. J. Magliochetti, «An in vitro assessment of the flow characteristics of spiral-ridged and smooth-walled JJ ureteric stents,» *BJU International*, vol. 85, nº 6, pp. 628-631, 2001.

[41] M. D. Dunn, A. J. Portis, S. A. Kahn, Y. Yan, A. Shalhav, A. M. Elbahnasy, E. Bercowsky, D. Hoenig, S. Wolf, E. McDougall y R. Clayman, «Clinical Effectiveness of New Stent Design: Randomized Single-Blind Comparison of Tail and Double-Pigtail Stents,» *Hournal of Endourology*, vol. 14, nº 2, pp. 195-202, 2000.

[42] B. Vogt, A. Desgrippes y F.-N. Desfemmes, «Changing the double-pigtail stent by a new suture stent to improve patient's quality life: a prospective study,» *World Journal of Urology*, vol. 33, nº 8, pp. 1061-1068, 2014.

[43] A. Farouk, A. Tawfick, M. Hasan, A. A. Abuftira y W. Maged, «Can Magnitip double-J Stent Serve as a Substitute for a Standard double-J Stent?,» *Turkish Journal of Urology,* vol. 45, nº 6, pp. 437-443, 2019.

[44] H. K. Park, S. H. Paick, H. G. Kim, Y. S. Lho y S. Bae, «The Impact of ureteral stent type on patient symptoms as determined by the ureteral stent symptom questionnaire: a prospective, randomized, controlled study.,» *Journal of Endourology,* vol. 29, nº 3, pp. 367-371, 2015.

[45] A. Brewer, A. Elbahnasy, E. Bercowsky, K. Maxwell, A. Shalhav, S. Kahn, E. McDougall y R. Clayman, «Mechanism of ureteral stent flow: a comparative in vivo study,» *Journal of endourology,* vol. 13, nº 4, pp. 269-271, 1999.

[46] K. Barrett, K. Foell , A. Lantz, M. Ordon, J. Y. Lee, K. T. Pace y R. J. D. Honey, «Best Stent Length Predicted by Simple CT Measurement Rather than Patient Height,» *Journal of Endourology,* vol. 30, nº 9, pp. 1029-1032, 2016.

[47] R. Damiano, R. Autorino, M. De Sio, F. Cantiello, G. Quarto, S. Perdonà, R. Sacco y M. D'Armiento, «Does the size of ureteral stent impact urinary symptoms and quality of life? A prospective randomized study,» *European Urology,* vol. 48, nº 4, pp. 673-678, 2005.

[48] A. Cubuk, F. Yanaral, F. Ozgor, M. Savun, H. Ozdemir, A. Erbin, B. Yuksel y O. Sarilar, «Comparison of 4.8 Fr and 6 Fr ureteral stents on stent related symptoms following ureterorenoscopy: A prospective randomized controlled trial,» *Kaohsiung Journal of Medical Sciencrr.*

[49] G. Astroza, M. Catalán, L. Consigliere, T. Selman, J. Salvado y F. Rubilar, «Is a ureteral stent required afetr use of ureteral access sheat in presented patients who undergo flexible ureteroscopy?,» *Central European Journal of Urology,* vol. 70, nº 1, pp. 88-92, 2016.

[50] F. Torricelli, S. De, B. Hinck, M. Noble y M. Monga, «Flexible ureteroscopy with a ureteral access sheath: when to stent?,» *Journal of Urology,* vol. 83, pp. 278-281, 2014.

[51] W. Sirithanaphol, S. Jitpraphai, T. Taweemonkongsap, C. Nualyong y E. Chotikawanich, «Ureteral stenting after flexible ureterorenoscopy with ureteral access sheat; is it really needed?: a prospective randomized study,» *J Med Assoc Thail,* Vols. %1 de %2174-178, p. 100, 2017.

[52] R. C. Calvert, K. Y. Wong, S. V. Chitale, S. O. Irving, M. Nagarajan, C. S. Biyani, A. J. Browning, J. G. Young, A. G. Timoney, F. X. Keely Jr y N. A. Burgess, «Multi-length or 24 cm ureteric stent? A multicentre randomised comparison of stent-related symptoms using a validated questionnaire,» *BJU International,* vol. 111, nº 7, pp. 1099-1104, 2013.

[53] H. B. Joshi, N. Newns, A. Stainthorpe, R. P. MacDonagh, F. X. Keeley y A. G. Timoney, «Ureteral Stent Symptom Questionnaire: Development and validation of a multidimensional quality of life measure,» *The Journal of Urology,* vol. 169, nº 3, pp. 1060-1064, 2003.

[54] J. E. Lingeman, G. M. Preminger, E. R. Goldfischer y A. E. Krambeck, «Assessing the impact of ureteral stent design on patient comfort,» *Hournal of Urology,* vol. 181, nº 6, pp. 2581-2587, 2009.

[55] M. J. C. R. Gibbons RP, «Experience with indwelling silicone rubber ureteral catheters,» *Journal of Urology,* vol. 111, nº 5, pp. 594-599, 1974.

[56] F. RP, «Experience with new double J ureteral catheter stent,» *Journal of Urology,* vol. 167, nº 2, pp. 1135-1138, 1978.

[57] D. L. Anderson, Jr y J. T. Maerzke, «Spiral Ureteral Stent». United States of America Patente 4,813,925, 21 March 1989.

[58] E. Liatsikos, D. Hom, C. Z. Dinlec, R. Kapoor, M. Alexianu, P. Yohannes y A. D. Smith, «Tail stent versus re-entry tube: a randomized comparison after percutaneous stone extraction,» *Adult Urology,* vol. 59, nº 1, pp. 15-19, 2002.

[59] B. Moskovitz, S. Halamachi y O. Nativ, «A New Self-Expanding, Large-Caliber Ureteral Stent: Results of a Multicenter Experience,» *Journal of Endourology,* vol. 26, nº 11, pp. 1523-1527, 2012.

[60] R. MC, M. MS, R. M y H. P, «Magnetic ureteral stent removal without cytoscopy: a randomized controlled trial,» *Journal of Endourology,* vol. 31, nº 8, pp. 762-766, 2017.

[61] S. P. Gorman, C. P. Garvin, F. Quigley y D. S. Jones, «Design and validation of a dynamic flow model simulating encrustation of biomaterial in the urinary tract,» *Journal of Pharmacy and Pharmacology,* vol. 55, nº 4, pp. 461-468, 2003.

[62] B. H. Chew, K. A. Rebullar, D. Harriman, E. McDougall, R. Paterson y D. Lange, «Percuflex helical ureteral stents significantly reduce patient analgesic Requirements compared to control stents.,» *Journal of Endourology,* vol. 31, nº 12, pp. 1321-1326, 2017.

[63] G. M. Lennon, J. A. Thornhill, P. A. Sweeney, R. Grainger, T. E. McDermott y M. R. Butler, «'Firm' versus 'Soft' double pigtail ureteric stents: a randomised blind comparative trial,» *European Urology,* vol. 28, nº 1, pp. 1-5, 1995.

[64] H. B. Joshi, S. V. Chitales, M. Nagarajan, S. O. Irving, A. J. Browning, C. S. Biyani y N. A. Burgess, «Prospective randomized single-blind comparison of ureteral stents composed of firm and soft polymer,» *The Journal of Urology,* vol. 174, nº 6, pp. 2303-2306, 2005.

[65] M. Arshad, S. S. Shah y M. H. Abbasi, «Applications and complications of polyurethane stenting in urology,» *Journal of Ayub Medical College,* vol. 18, nº 2, pp. 69-72, 2006.

[66] M. Marx, M. A. Bettmann, S. Bridge, G. Brodsky, L. Boxt y J. Richie, «The effects of various indwelling ureteral catheter materials on the normal canine ureter,» *The Journal of Urology,* vol. 139, nº 1, pp. 180-185, 1988.

[67] R. Damiano, O. Andrea, C. Espocito, M. De Sio, R. Autorino y M. D'Armiento, «Early and Late Complicationes of Double Pigtail Ureteral Stent,» *Urologia Internationalis,* vol. 69, pp. 136-140, 2002.

[68] X. Wang, H. Shan, J. Wang, Y. Hou, J. Ding, Q. Chen, J. Guan, C. Wang y X. Chen , «Characterization of nanostructured ureteral stent with gradient degradation in a porcine model,» *International Journal of Nanomedicine,* vol. 10, pp. 3055-3064, 2015.

[69] S. P. Groman, M. M. Tunney, P. F. Keane, K. Van Bladel y B. Bley, « Characterization and assessment of a novel poly(ethylene oxide)/polyurethane composite hydrogel as a ureteral stent biomaterial,» *Journal of Biomedical Materials Reasearch,* vol. 39, nº 4, pp. 642-649, 1997.

[70] F. Desgrandchamps, F. Moulinier, M. Daudon, P. Teillac y A. Le Duc, «An in vitro comparison of urease-induced encrustation of JJ stents in human urine,» *British journal of urology,* vol. 79, nº 1, pp. 24-27, 1997.

[71] T. John, A. Rajpurkar, G. Smith, M. Fairfax y J. Triest, «Antibiotic pretreatment of hydrogel ureteral stent,» *Journal of Endourology,* vol. 21, nº 10, 2007.

[72] M. M. Tunney y S. P. Gorman, «Evaluation of a poly(vinyl pyrollidone)-coated biomaterial for urological use,» *Biomaterials,* vol. 23, pp. 4601-4608, 2002.

[73] F. Cauda, V. Cauda, C. Fiori , B. Onida y E. Garrone, «Heparin Coating on Ureteral Double J Stents Prevents Encrustations: An in vivo case study,» *Journal of Endourology,* vol. 22, nº 3, 2008.

[74] P. Tenke, C. R. Riedl, G. L. Jones, G. J. Williams, D. Stickler y E. Nagy, «Bacterial biofilm formation on urological devices and heparin coating as preventive strategy,» *International Journal of Antimicrobial Agents,* vol. 23, pp. 67-74, 2004.

[75] P. Hildebrandt, M. Sayyad, A. Rzany, M. Schaldach y H. Seiter, «Prevention of surface encrustation of urological implants by coating with inhibitors,» *Biomaterials,* vol. 22, nº 5, pp. 503-507, 2001.

[76] C. R. Riedl, M. Witkowski, E. Plas y H. Pflueger, «Heparin coating reduces encrustation of ureteral stents: a preliminary report,» *International journal ofantimicrobial agents,* vol. 19, nº 6, pp. 507-510, 2002.

[77] D. Lange, C. Elwood, K. Choi, K. Hendlin, M. Monga y B. H. Chew, «Uropathogen interaction with the surface of urological stents using different surface properties,» *The Journal of Urology,* vol. 182, nº 3, pp. 1194-1200, 2009.

[78] P. Zupkas, C. L. Parsons, C. Percival y M. Monga, «Pentosanpolysulfate coating of silicone reduces encrustation,» *Journal of Endourology,* vol. 14, nº 6, pp. 483-488, 2000.

[79] N. Laube, L. Kleinen, J. Bradenahl y A. Meissner, «Diamond-like carbon coatings on ureteral stents - A new strategy for decreasing the formation of crystalline bacterial biofilms?,» *Journal of Urology,* vol. 177, nº 5, pp. 1923-1927, 2007.

[80] L. Mao, L. Shen, J. Chen, X. Zhang, M. Kwak, Y. Wu, R. Fan, L. Zhang, J. Pei, G. Yuan, C. Song, J. Ge y W. Ding, «A promising biodegradable magnesium alloy suitable for clinical vascular stent application,» *Scientific reports,* vol. 7, nº 46343, 2017.

[81] L. Wang, G. Yang, H. Vie y F. Chen, «Prospects for the research and application of biodegradable ureteral stents: From brench to bedside,» *Journal of Biomaterials Science, Polymer Edition,* pp. 1-16, 2018.

[82] R. S. Kirby, S. R. Heard, P. Miller, I. Eardley, S. Holmes, J. Vale, J. Bryan y S. Liu, «Use of the ASI titanium stent in the managemetn of bladder outflow obstruction due to benign prostatic hyperplasia,» *The Journal of Urology,* vol. 148, nº 4, pp. 1195-1197, 1992.

[83] H.-Y. Song, H. Park, T.-S. Suh, G.-Y. Ko, T.-H. Kim, E.-S. Kim y T. Park, «Recurrent Traumatic Urethral Strictures near the External Sphincter: Treatment with a Covered, Retrievable, Expandable Nitinol Stent-Initial Results,» *Radiology,* vol. 226, nº 2, pp. 433-440, 2003.

[84] G. I. Papadopoulos, S. Middela, S. J. Srirangam, C. A. Szczesniak y P. Rao, «Use of Memokath 051 Metallic Stent in the managemente of Ureteral Strictures: A single-Center Experience,» *Urologia Internationalis,* vol. 84, nº 3, pp. 286-291, 2010.

[85] P. Klarskov, J. Nordling y J. B. Nielsen, «Experience with Memokath 051 Ureteral Stent,» *Scandinavian Journal of Urology and Nephrology,* vol. 39, nº 2, pp. 169-172, 2005.

[86] K. J. Chung, B. H. Park, B. Park, J. H. Lee, W. J. Kim, M. Baek y D. H. Han, «Efficay and Safety of a novel, double-layared, coated, self-expandable metallic mesh stent (Uventa™) in malignant ureteral obstructions,» *Journal of Endourology,* vol. 27, nº 7, pp. 930-935, 2013.

[87] K. S. Kim, S. Choi, Y. S. Choi, W. J. Bae, S.-H. Hong, J. Y. Lee, S. W. Kim, T.-K. Hwang y H. J. Cho, «Comparison of efficacy and safety between a segmental thermo-expandable metal alloy spiral stent (Memokath 051) and a self-expandable coverde metallic stent (Uventa) in the management of ureteral obstructions,» *Journal of Laparoendoscopic & Advanced Surgicatl Techniques,* vol. 24, nº 8, pp. 550-555, 2014.

[88] M. Kim, B. Hong y H. K. Park, «Long-term outcomes of double-layered polytetrafluoroethylene membrane-coveredd self-expandable segmental metallic stents (Uventa™) in patients with chronic ureteral obstructions: is it really safe?,» *Journal of Endourology,* vol. 30, nº 12, pp. 1339-1346, 2016.

[89] A. D. Benson, B. F. Schwartz y E. R. Taylor, «Metal ureteral stent for benign and malignant ureteral obstruction,» *Journal of urology,* vol. 185, nº 6, pp. 2217-2222, 2011.

[90] E. Liatsikos, P. Kallidonis, I. Kyriazis, C. Constantinidis, K. Hendlin, J.-U. Stolzenburg, D. Karnabatidis y D. Siablis, «Ureteral Obstruction: Is the Full Metallic Double-Pigtail Stent the Way to Go?,» *European Urology,* vol. 57, nº 3, pp. 480-487, 2010.

[91] J. Y. Lock, M. Draganov, A. Whall, S. Dhillon, S. Upadhyayula, V. I. Vullev y H. Liu, «Antimicrobial properties of biodegradable magnesium for next generation ureteral stent applications,» *2012 Annual International Conference of the IEEE Engineering in Medicine and Biology Society,* 2012.

[92] S. Zhang, Y. Bi, J. Li, Z. Wang, J. Yan, J. Song, H. Sheng, H. Guo y Y. Li, «Biodegradation behavior of magnesium and ZK60 alloy in artificial urine and rat models,» *Bioactive Materials,* pp. 1-10, 2017.

[93] E. Mostaed, M. Sikora-Jasinska, A. Mostaed, S. Loffredo, A. Demir, B. Previtali, D. Mantovani, R. Beanland y M. Vedani, «Novel Zn-based alloys for biodegradable stent applications: Design, development and in vitro degradation,» *Journal of the Mechanical Bahavior of Biomedical Materials,* vol. 60, pp. 581-602, 2016.

[94] D. Hernández-Escobar, S. Champagne, H. Yilmazer, B. Dikici, C. J. Boehlert y H. Hermawan, «Current status and perspectives of zinc-based absorbable alloys for biomedical applications,» *Acta Biomaterialia,* vol. 97, pp. 1-22, 2019.

[95] R. Sharif, P. Thomas, P. Zalewski y M. Fenech, «The role of zinc in genomic stability,» *Mutation Research/Fundamental and Molecular Mechanisms of Mutagenesis,* vol. 733, pp. 111-121, 2012.

[96] B. B. McAllister y R. H. Dyck, «A new role for zinc in the brain,» *eLife,* vol. 6, 2017.

[97] P. Christian y K. P. West, «Interactions between zinc and vitamin A: an update,» *The American Journal of Clinical Nutrition,* vol. 68, nº 2, pp. 431-441, 1998.

[98] T. Kambe, T. Tsuji, A. Hashimoto y N. Itsumura, «The Physiological, Biochemical, and Molecular Roles of Zinc Transporters in Zinc Homeostasis and Metabolism,» *Physiological reviews,* vol. 95, nº 3, pp. 749-784, 2015.

[99] Agency for Toxic Substances and Disease Registry Division of Toxicology and Environmental Medicine, «Toxicological Profile for Zinc,» Atlanta, GA, USA, 2005.

[100] J. Nriagu, «Zinc Toxicity in Humans,» de *Encyclopedia of Environmental Health*, Elseiver, 2019, pp. 500-508.

[101] G. D. Considine, Van Nostran's Encyclopedia of Chemistry, Hoboken, New Jersey: Wiley-Interscience, 2005.

[102] M. Weller , T. Overton, F. Armstrong y J. Rourke, «The d-block elements,» de *Inorganic Chemistry*, Oxford University Press, 2018, p. 563.

[103] Government of Canada, «Natural Resources Canada,» 27 11 2019. [En línea]. Available: https://www.nrcan.gc.ca/our-natural-resources/minerals-mining/zinc-facts/20534#L3. [Último acceso: 03 11 2020].

[104] Y. Zhanga, Y. Yan, X. Xu, Y. Lu, L. Chen, D. Li, Y. Dai, Y. Kang y K. Yu, «Investigation on the microstructure, mechanical properties, in vitro degradation behavior and biocompatibility of newly developed Zn-0.8%Li-(Mg, Ag) alloys for guided bone regeneration,» *Materials Science & Engineering C,* vol. 99, pp. 1021-1034, 2019.

[105] P. Sotoudeh Bagha, S. Khaleghpanah, S. Sheibani, M. Khakbiz y A. Zaker, «Characterization of nanostructured biodegradable Zn-Mn alloy synthesized by mechanical alloying,» *Journal of Alloys and Compounds,* 2017.

[106] Z. Tang, J. Niu, H. Huang, H. Zhang, J. Pei, J. Ou y G. Yuan, «Potential biodegradable Zn-Cu binary alloys developed for cardiovascular implant applications,» *Journal of the Mechanical Behavior of Biomedical Materials,* vol. 72, pp. 182-191, 2017.

[107] C. Xiao, L. Wang, Y. Ren, S. Sun, E. Zhang, C. Yan, Q. Liu, X. Sun, F. Shou, J. Duan, H. Wang y G. Qin, «Indirectly extruded biodegradable Zn-0.05wt%Mg alloy with improved strength and ductility: In vitro and in vivo studies,» *Journal of Materials Science & Technology,* vol. 34, nº 9, pp. 1618-1627, 2018.

[108] S. Zhao, J.-M. Seitz, R. Eifler, H. J. Maier, R. J. Guillory, E. Earley, A. Drelich, J. Goldman y J. Drelich, «Zn-Li alloy after extrusion and drawing: Structural, mechanical

characterization, and biodegradation in abdominal aorta of rat,» *Materials Science and Engineering C,* vol. 76, pp. 301-312, 2017.

[109] L. Wang, Y. He, H. Zhao, H. Xie, S. Li, Y. Ren y G. Qin, «Effect of cumulative strain on the microstructural and mechanical properties of Zn-0.02wt.%Mg alloy wires during room-temperature drawing process,» *Journal of Alloys and Compounds,* pp. 949-957, 2018.

[110] H. R. Bakhsheshi-Rad, E. Hamzah, H. T. Low, M. Kasiri-Asgarani, S. Farahany, E. Akbari y M. H. Cho, «Fabrication of biodegradable Zn-Al-Mg alloy: Mechanical properties, corrosion behavior, cytotoxicity and antibacterial activities,» *Materials Science and Engineering C,* vol. 219, nº 73, p. 215, 2017.

[111] J. Kubásek, D. Vojtěch, E. Jablonská, I. Pospíšilová, J. Lipov y T. Ruml, «Structure, mechanical characteristics and in vitro degradation, cytotoxicity, genotoxicity and mutagenicity of novel biodegradable Zn–Mg alloys,» *Materials Science and Engineering C,* vol. 58, pp. 24-35, 2016.

[112] D. Vojtech, J. Kubásek, J. Šerák y P. Novák, «Mechanical and corrosion properties of newly developed biodegradable Zn-based alloys for bone fixation,» *Acta Biomaterialia,* vol. 7, nº 9, pp. 3515-3522, 2011.

[113] G. Katarivas Levy, A. Leon, A. Kafri, Y. Ventura, J. W. Drelich, J. Goldman, R. Vago y E. Aghion, «Evaluation of biodegradable Zn-1%Mg and Zn-1%Mg-0.5%Ca alloys for biomedical applications,» *Journal of Materials Science,* vol. 28, p. 174, Materials in Medicine.

[114] A. Jarzębska, M. Bieda, J. Kawałko, . Ł. Rogal, P. Koprowski, K. Sztwiertnia, W. Pachla y M. Kulczyk, «A new approach to plastic deformation of biodegradable zinc alloy with magnesium and its effect on microstructure and mechanical properties,» *Materials Letters,* 2018.

[115] J. Kubasek y D. Vojtech, «Zn-based alloys as an alternative biodegradable materials,» *Proc. Metal,* p. 23–25 , 2012.

[116] H. Gong, K. Wang, R. Strich y J. G. Zhou, «In vitro biodegradation behavior, mechanical properties, and cytotoxicity of biodegradable Zn–Mg alloy,» *Journal of Biomedical Materials Research Part B,* vol. 103, nº 8, pp. 1632-1640, 2015.

[117] H. Li, H. Yang, Y. Zheng, F. Zhou, K. Qiu y X. Wang, «Design and characterizations of novel biodegradable ternary Zn-based alloys with IIA nutrient alloying elements Mg, Ca and Sr,» *Materials & Design,* vol. 83, pp. 95-102, 2015.

[118] X. Liu, J. Sun, F. Zhou, Y. Yinghon, . R. Chang, K. Qiu, . Z. Pu, L. Li y . Y. Zheng, «Micro-alloying with Mn in Zn-Mg alloy for future biodegradable metals application,» *Materials & Design,* vol. 94, pp. 95-104, 2016.

[119] X. Liu, J. Sun, Y. Yang, F. Zhou, Z. Pu, L. Li y Y. Zheng, «Microstructure, mechanical properties, in vitro degradation behavior and hemocompatibility of novel Zn-Mg-sr alloys as biodegradable metals,» *Materials Letters,* 2015.

[120] C. Shen, X. Liu, B. Fan, P. Lan, F. Zhou, X. Li, H. Wang, X. Xiao, L. Li, S. Zhao, Z. Guo, Z. Pujie y Y. Zheng, «Mechanical properties, in vitro degradation behavior,

hemocompatibility and cytotoxicity evaluation of Zn–1.2Mg alloy for biodegradable implants,» *RSC Advances*, vol. 6, pp. 86410-86419, 2016.

[121] M. S. Dambatta, S. Izman, D. Kurniawan y H. Hermawan, «Processing of Zn-3Mg alloy by equal channel angular pressing for biodegradable metal implants,» *Journal of King Saud University*, vol. 29, nº 4, pp. 455-461, 2017.

[122] P. Li, C. Schille, E. Schweizer, E. Kimmerle-Mûller, F. Rupp, X. Han, A. Heiss, A. Richter, C. Legner, u. E. Klotz, J. Geis-Gerstorfer y L. Scheideler, «Evaluation of a Zn–2Ag–1.8Au–0.2V Alloy for Absorbable Biocompatible Materials,» *Materials*, vol. 13, 2019.

[123] M. Sikora-Jasinska, E. Mostaed, E. Mostaed, R. Beanland, D. Mantovani y M. Vedani, «Fabrication, mechanical properties and in vitro degradation behavior of newly developed Zn-Ag alloys for degradable implant applications,» *Materials Science and Engineering C*, vol. 77, pp. 1170-1181, 2017.

[124] P. Li, C. Schille, E. Schweizer, F. Rupp, A. Heiss, C. Legner, U. E. Klotz, J. Geis-Gerstorfer y L. Scheideler, «Mechanical Characteristics, In Vitro Degradation, Cytotoxicity, and Antibacterial Evaluation of Zn-4.0Ag Alloy as a Biodegradable Material,» *International Journal od Molecular Sciences*, vol. 19, 2018.

[125] H. Armano, K. Miyake, A. Hinoki, K. Yokota, F. Kinoshita, A. Nakazawa, Y. Tanaka, Y. Seto y H. Uchida, «Novel zinc alloys for biodegradable surgical staples,» *World Journal of Clinical Cases*, vol. 8, nº 3, pp. 504-516, 2020.

[126] J. Lin, X. Tong, Z. Shi, . D. Zhang, L. Zhang, K. Wang, A. Wei, L. Jin, J. Lin, Y. Li y C. Wen, «A biodegradable Zn-1Cu-0.1Ti alloy with antibacterial properties for orthopedic applications,» *Acta Biomaterialia*, 2020.

[127] R. Yue, H. Huang, G. Ke, H. Zhang, J. Pei, G. Xue y G. Yuan, «Microstructure, mechanical properties and in vitro degradation behavior of novel Zn-Cu-Fe alloys,» *Materials Characterization*, vol. 134, pp. 114-122, 2017.

[128] Z. Tang, H. Huang, J. Niu, L. Zhang, H. Zhang, J. Pei, J. Tan y G. Yuan, «Design and characterizations of novel biodegradable Zn-Cu-Mg alloys for potential biodegradable implants,» *Materials & Design*, 2016.

[129] J. Niu, Z. Tang, H. Huang, J. Pei, H. Zhang, G. Yuan y W. Ding, «Research on a Zn-Cu alloy as a biodegradable material for potential vascular stents application,» *Materials Science and Engineering C*, vol. 69, pp. 407-413, 2016.

[130] J. Niu, Z. Tang, H. Huang, J. Pei, H. Zhang, G. Yuan y W. Ding, «Research on a Zn-Cu alloy as a biodegradable material for potential vascular stents application,» *Materials Science and Engineering C*, vol. 69, pp. 407-413, 2016.

[131] S. Sun, Y. Ren, L. Wang, B. Yang, H. Li y G. Qin, «Abnormal effect of Mn addition on the mechanical properties of as-extruded Zn alloys,» *Materials Science &Engineering A*, 2017.

[132] Z.-Z. Shi, J. Yu, X.-F. Liu y L.-N. Wang, «Fabrication and characterization of novel biodegradable Zn-Mn-Cu alloys,» *Journal of Materials Science & Technology,* vol. 34, pp. 1008-1015, 2018.

[133] S. Zhao, C. McNamara, P. Bowen, N. Verhun, J. P. Braykovich, J. Goldman y J. Drelich, «Structural Characteristics and In Vitro Biodegradation of a Novel Zn-Li Alloy Prepared by Induction Melting and Hot Rolling,» *Metallurgical and Materials Roling,* vol. 48, nº 3, pp. 1204-1215, 2017.

[134] X. G. Zhang, Corrosion and electrochemistry of Zinc, Mississauga, Ontario, Canada : Springer Science + Business Media, 1996.

[135] K. Tôrne, M. Larsson, A. Norlin y J. Weissenrieder, «Degradation of zinc in saline solutions, plasma and whole blood,» *Society for Biomaterials,* vol. 104, nº 6, pp. 1141-1151, 2015.

[136] S. Champagne, E. Mostaed, F. Safizadeh, E. Ghali, M. Vedani and H. Mermawan, "In Vitro Degradation of Absorbable Zinc Alloys in Artificial Urine," *Materials,* vol. 12, no. 295, 2019.

[137] Y. Okamura, N. Hinata, T. Hoshiba, T. Nakatsuji, N. Ikeo, J. Furukawa, K. Harada, Y. Nakano, T. Fukumoto, T. Mukai y M. Fujisawa, «Development of bioabsorbable zinc-magnesium alloy wire and validation of its application to urinary tract surgeries,» *World Journal of Urology,* 2020.

[138] X. Tong, D. Zhang, X. Zhang, Y. Su, Z. Shi, K. Wang, J. Lin, Y. Li, J. Lin y C. Wen, «Microstructure, mechanical properties, biocompatibility, and in vitro corrosion and degradation behavior of a new Zn–5Ge alloy for biodegradable implant materials,» *Acta Biomaterialia,* 2018.

[139] Y. Zpu, X. Chen y B. Chen, «Effects of Ca concentration on degradation behavior of Zn-x Ca alloys in Hank's solution,» *Materials Letters,* 2018.

[140] A. Barhoum y A. S. Hamdy Makhlouf, «Evaluation of Self-Healing Activity of Micro- and Nanocapsules filled with inhibitors. Electrochemical Techniques.,» de *Fundamentals of Nanoparticles: Classifications, Synthesis Methods, Properties and Characterization*, Elsevier, 2018, pp. 541-543.

[141] D. A. Jones, Principles and Prevention of Corrosion, Prentice-Hall, 1996.

[142] S. Papavinasam , «Electrochemical polarization techniques for corrosion monitoring,» de *Techniques for corrosion monitoring*, Woodhead Publishing Series in Metals and Surface Engineering, 2008, pp. 49-85.

[143] K. Kakaei, M. Esrafili y A. Ehsani, «Graphene and Anticorrosive Properties. Polarization Techniques and Tafel Extrapolation.,» de *Graphene Surfaces: Particles and Catalysts*, Interface Science and Technology, Elsevier, 2019, pp. 306-309.

[144] ASTM International, «ASTM G102 - Standard Practice for Calculation of Corrosion Rates and Related Information from Electrochemical Measurements,» 1994.

[145] D. J. Griffiths, «Flow of Urine Through the Ureter: A Collapsible, Muscular Tube Undergoing Peristalsis,» *Journal of Bioechanical engineering,* vol. 111, nº 3, pp. 206-211, 1989.

[146] A. Majid, N. Ahmed, M. A. Khan, M. Rashid, Z. A. Umar y M. A. Baig, «Synthesis and characterization of Zn/ZnO microspheres on indented sites of silicon substrate,» *Materials Science-Poland,* vol. 36, nº 3, pp. 501-508, 2018.

[147] M. Caligari Conti, D. Aquílina , C. Paternoster, D. Vella, E. Sinagra, D. Mantovani, G. Cassar, P. Schembri Wismayer y J. Buhagiar, «Influence of cold rolling on in vitro cytotoxicity and electrochemical behaviour of an fe-Mn-C biodegradable alloy in physiological solutions,» *Heliyon,* vol. 4, 2018.

[148] A. Kafri, S. Ovadia, J. Goldman, J. Drelich y E. Aghion, «The Suitability of Zn-1.3%Fe Alloy as a Biodegradable Implant Material,» *Metals,* vol. 8, 2018.

[149] N. Van Phuong y S. Moon, «Comparative corrosion study of zinc phosphate and magnesium phosphate conversion coatings on AZ31 Mg alloy,» *Materials Letters,* vol. 122, nº 1, pp. 341-344, 2014.

[150] R. Selvaraju, A. Raja y G. Thiruppathi, «FT-IR spectroscopic, thermal analysis of human urinary stones and their characterization,» *Spectrochimica Acta Part A: Molecular and Biomolecular Spectroscopy,* vol. 137, pp. 1397-1402, 2015.

[151] S. Falahatkar, «Missed Ureteral Stents and Related Problems,» *Nephro-Urology Monthly,* vol. 5, pp. 777-778, 2013.

[152] A. Jairath, A. Ganpule y M. Desai, «Percutaneous nephrostomy step by step,» *Mini-invasive Surg,* vol. 1, pp. 180-185, 2017.

[153] National Kideny Foundation, «Nephrectomy,» July 2009. [En línea]. Available: https://www.kidney.org/atoz/content/nephrectomy. [Último acceso: 20 July 2020].

[154] Oxford Centre for Evidence-Based Medicine, «Levels of Evidence,» March 2009. [En línea]. Available: https://www.cebm.net/2009/06/oxford-centre-evidence-based-medicine-levels-evidence-march-2009/. [Último acceso: 12 June 2020].

[155] P. L. Marino, «Vascular access,» de *The ICU book*, Lippincott Williams & Wilkins, 2007, p. 108.

[156] World Health Organization, «WHO Definition of Palliative,» [En línea]. Available: https://www.who.int/cancer/palliative/definition/en/. [Último acceso: 16 06 2020].